Examination of Field Electron Emission from Knife-Edge Structures

by

Nishant Sule

A thesis submitted in partial fulfillment of

the requirements of the degree of

Master of Science

(Electrical Engineering)

at the

UNIVERSITY OF WISCONSIN-MADISON

2009

Abstract

This thesis reports the experimental and modeling research carried out on field and thermal emission from knife-edge structures. Field emission arises from electron emission from a surface under the influence of intense electric fields by the process of quantum mechanical tunneling through the potential barrier at the material-vacuum interface. The field emission experiments were done on the Madison Cathode Experiment (MACX) setup with cathodes fabricated with raised vanes or knife-edges. Measurements of emission current as a function of applied voltage, anode-cathode spacing and temperature were recorded using an amplifier developed for these experiments and analysis of the experimental data was done using Fowler-Nordheim theory as well as thermal-field emission processes. Cathode parameters such as work function (ϕ), field enhancement factor (β) and the effective emitting area (A) are extracted for the copper knife edge (CKE) cathodes making use of thermal and field emission data. The ranges of cathode parameters thus obtained are, $\phi \approx 2.96$–4.7 eV, $\beta \approx 400$–440 and $A \approx 6.3$–6.66×10^{-7} m^2. Evidence of space charge limited emission current is also obtained for these CKE cathodes. Investigations of field emission from lanthanum hexaboride (LaB_6) thin films (~ 300 nm) sputter deposited on these CKE cathodes with a titanium adhesion layer on copper are also reported. These thin films of LaB_6 have a low work function (~ 2.6 eV) and are expected to enhance the emission current density from the CKE cathodes. However, the experiments obtain a lower emission current density than bare copper and nonlinear field emission current variations from these LaB_6 films at elevated temperatures ($\sim$200℃). A hypothesis based on electron transport in the copper metal and the LaB_6 thin film is presented to explain these observations. In conclusion, some future experiments are suggested to further investigate field emission from CKE cathodes as well as field emission properties with differing LaB_6 thickness thin films on CKE structures.

Acknowledgements

It is with my deepest appreciation that I acknowledge my advisor, Dr. John E. Scharer, for his support, encouragement and freedom to pursue my own ideas in this research project. His guidance has been invaluable and he has taught me to be rigorous in research. I am also equally thankful to Dr. John H. Booske, without whose advise, ideas and suggestions I wouldn't have completed this project. This work is greatly dedicated to them for their support.

This work has been supported by AFOSR by a USDOD MURI05 grant on the Nano physics of High Current Density Cathode and Breakdown. I would like to thank them for the financial support during the project. A special acknowledgment to all the students in Dr. Scharer's and Dr. Booske's group for their constant help and motivation. They have all helped me a lot. Thanks to all my friends in Madison, Wisconsin for making my stay here enjoyable and productive.

I also deeply thank my family, my elder brother, Nitesh and his wife Preeti, for their unconditional support and affection. My most special thanks to my loving fiancée, Rashmi, for being understanding, supporting and cheering me up in my moments of frustration. A big thanks to all my friends back in India for always believing in me and wishing me the best.

Lastly, and most importantly, I wish to thank my parents who have raised me, taught me, loved me and unequivocally supported me in all my endeavors. To them I dedicate this thesis.

Contents

List of Figures

List of Tables

Chapter 1

Introduction & Background Theory

Field emission is a phenomenon that has a vast technological context. From the time this phenomenon has been understood, researchers have found novel applications utilizing it. My thesis is on the experimental study of field emission from knife-edge structured cathodes. This chapter serves as an introduction to field electron emission and provides background theoretical knowledge essential to understand the experiments and analysis. There are different mechanisms through which an electron inside a material can be emitted, such as, photo electron emission, thermionic emission, secondary electron emission and field electron emission. The focus of this chapter would be on field emission, however a description of thermal emission is also provided along with thermal-field emission since it is relevant for experiments described later in the thesis. This chapter also describes the numerous practical applications for field electron emission from the past, present and those envisioned for the future.

1.1 Electron Emission Theories

Electron emission can be defined as the liberation of electrons from the surface of a material due to external energy transferred to the electrons. This phenomenon is most frequently observed in metals as there are more free electrons which can gain external energy. The minimum energy (usually measured in electron volts) needed to remove an electron from the Fermi level in a metal to a point an infinite distance away from the surface is called the work function of that surface [1]. There are various mechanism through which an electron inside a metal, can be emitted outside its surface. Based on the source of energy for the emitted electron, the mechanisms are classified as photo emission (energy from light), thermionic emission (energy from heat), secondary electron emission (kinetic energy from another electron) and field emission (energy from electric field). The mechanism relevant to this research work are of course field electron emission and thermal-field emission. A combined thermal-field emission description is employed when emission is due to both a high temperature and under influence of an electric field [2]. These two relevant electron emission mechanism theories will be discussed in detail below.

1.1.1 Field Electron Emission

The mechanism of field emission has no analogue in the other electron emission mechanisms since it is based on the phenomenon of quantum mechanical tunneling. It was observed a long time back in 1897 by Wood [3] but was first explained correctly by R. Fowler and L. Nordheim [4] in 1928. Fowler-Nordheim (F-N) explained that electrons are emitted as they tunnel through a potential barrier that is lowered and narrowed due to presence of intense electric fields and derived the emission current density. Thus, according to the F-N 1D model, electrons arrive at the surface of a metal, which is assumed at 0 ℃, according to Fermi-Dirac statistics and penetrate

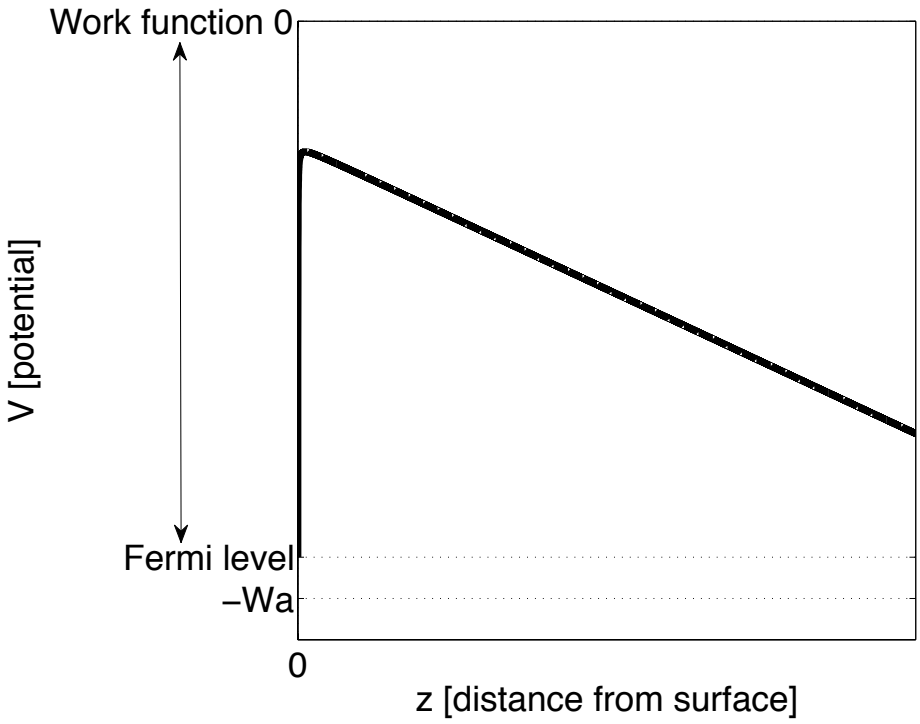

Figure 1.1: 1D Potential energy barrier for an electron near a metal surface

the potential barrier in front of the surface with a probability given by the Schödinger equation. The shape of the potential barrier is described by the electric field and the presence of image charges. Far outside the metal surface, ($z \to \infty$), in absence of an electric field, the potential energy is chosen to be zero. Inside the metal the electrons are assumed to have a constant effective potential energy $-W_a$. Then, in presence of an electric field, $\mathbf{E}$, the potential barrier is described by [5]

$$V(z) = -W_a \qquad \text{where} \quad z < 0, \tag{1.1}$$

$$= -\frac{e^2}{4z} - e\mathbf{E}z \qquad \text{where} \quad z > 0. \tag{1.2}$$

Figure 1.1 shows the one-dimensional potential energy barrier faced by an electron inside the metal, near the surface. The first term in equation 1.2 comes from the inclusion of image charges. Classical image charge correction is good approximation

since it is difficult to exactly calculate the electron potential at the surface from the appropriate exchange and correlation energy terms. The supply function of the electrons is taken from the Sommerfeld's theory of electrons in a metal and is equal to the number of electrons with energy within the range E to $E+dE$ whose z part of energy lies in the range W to $W+dW$, incident on the surface per second per area. Thus the supply function is given by [6]

$$N(W,E)dWdE = -\frac{4\pi m}{h^3}\frac{dWdE}{\exp\left[\frac{(E-\xi)}{kT}\right]+1} \tag{1.3}$$

This supply function is then multiplied by the barrier penetration probability or the transmission coefficient, $D(W)$, which is defined as the probability for an electron, with z part of energy equal to W, that will penetrate the potential barrier. This yeilds the number of electrons within the range W and $W+dW$ that emerge from the metal surface per second per unit area. $D(W)$ can be calculated using the WKB approximation [7]. For $W \ll V_{\max}$ (the apex of the potential barrier) and for the emission range $W \sim \xi$, where ξ is the Fermi energy, $D(W)$ is shown to be [6]

$$D(W) \cong \exp\left[\frac{-c+(W-\xi)}{d}\right] \tag{1.4}$$

$$\text{where} \qquad c = \frac{4(2m\phi^3)^{\frac{1}{2}}}{3\hbar e\mathbf{E}}v(y), \tag{1.5}$$

$$d = \frac{\hbar e\mathbf{E}}{2(2m\phi)^{\frac{1}{2}}t(y)}, \tag{1.6}$$

$$\text{and} \qquad y = \frac{(e^3\mathbf{E})^{\frac{1}{2}}}{\phi} \tag{1.7}$$

here, ϕ is the work function of the metal surface and $t(y)$ and $v(y)$ are slowly varying functions. Now, the number of electrons in the given energy range penetrating the barrier is given by $N(W,E)D(W)dWdE = P(W,E)dWdE$. The total energy distribution, $P(E)dE$ is then calculated by integrating over the energy range E to $-W_a$.

This integration is facilitated by setting the limit $-W_a$ equal to $-\infty$ to obtain

$$P(E)dE = \int_{W=E}^{-W_a} N(W,E)D(W)dWdE \tag{1.8}$$

$$= \frac{4\pi md}{h^3}\exp\left[-c-\frac{\xi}{d}\right] \times \frac{e^{E/d}}{\exp\left[\frac{E-\xi}{kT}\right]+1}dE \tag{1.9}$$

And, finally the total emitted current density is given by $e\int P(E)dE$[6]. Thus,

$$\mathbf{J} = e\int_{-\infty}^{\infty} P(E)dE = \frac{4\pi mde}{h^3}\exp\left[-c-\frac{\xi}{d}\right] \times \int_{-\infty}^{\infty} \frac{e^{E/d}}{\exp\left[\frac{E-\xi}{kT}\right]+1}dE \tag{1.10}$$

After some manipulations this can be put in standard form. The solution is valid only when $d > kT$. The reduced equation is then written as

$$\mathbf{J} = \frac{e^3\mathbf{E}^2}{8\pi h\phi t^2(y)} \times \exp\left[-\frac{8\pi(2m)^{\frac{1}{2}}\phi^{\frac{3}{2}}}{3he\mathbf{E}}v(y)\right]\frac{\pi kT/d}{\sin(\pi kT/d)} \tag{1.11}$$

For $T \to 0$, $\frac{\pi kT/d}{\sin(\pi kT/d)} = 1.$ and so

$$\mathbf{J} = \frac{A\mathbf{E}^2}{\phi t^2(y)}\exp\left[-\frac{Bv(y)\phi^{\frac{3}{2}}}{\mathbf{E}}\right] \tag{1.12}$$

$$\text{where} \qquad A = \frac{e^3}{8\pi h} \approx 1.541434 \times 10^{-6}\ \text{A eV V}^{-2} \tag{1.13}$$

$$\text{and} \qquad B = \frac{8\pi\sqrt{2m}}{3he} \approx 6.830890\ \text{eV}^{-3/2}\ \text{nm}^{-1} \tag{1.14}$$

Equation 1.12 is known as the standard F-N equation for current density due to cold field electron emission and the constants A (1.13) and B (1.14) are known as the first and second F-N constants.

A more generalized equation has been proposed in recent times that includes various physical correction factors. In the standard form of F-N equation, the slowly varying functions $t(y)$ and $v(y)$ are replaced by their approximate numerical values. This has been shown to under-predict $\mathbf{J}$ values, often by a factor of 100 [8]. Hence, in the general form, the functions $t^{-2}(y)$ and $v(y)$ are replaced by parameters, λ and μ, whose forms depend on the type of approximation made. The parameter λ

includes effects from the Tunneling pre-factor emerging from the JWKB treatment for calculating transmission probability $D(W)$. It also includes temperature effects and electronic band structure effects. The parameter μ contains information of the barrier shape [8]. The F-N equation has been successfully able to predict emission currents for a very large range of electric fields and current densities and works surprisingly well at non-zero temperature. However, this simple equation fails at very large current densities where space charge effects start to dominate as well as high temperatures and low fields where thermal emission dominates. The next section describes thermal-field emission in more detail.

1.1.2 Thermal Field Emission

Before describing the theory for thermal-field emission, it is more fitting to describe thermionic emission and then combine the above theory of field emission into it to form a general thermal-field emission theory.

Thermionic Emission

In thermionic emission, (and photoemission) as opposed to field emission, the potential barrier in not deformed, but the electrons are given sufficient energy to overcome the barrier. This energy comes from heating the metal until sufficient electrons acquire kinetic energies $\geq \phi + \xi$. The emission current density can be estimated by Richardson's Law [9] (also known as RLD equation)

$$\mathbf{J} = A_G T^2 \exp\left[-\frac{\phi}{kT}\right] \tag{1.15}$$

here, $A_G = \lambda_R A_0$ where λ_R is a material specific correction factor and A_0 is a universal constant given by

$$A_0 = \frac{4\pi m k^2 e}{h^3} = 1.20173 \times 10^6 \text{ A/m}^2 \text{ K}^2 \tag{1.16}$$

The derivation of this equation is less complex. The same supply function is used as in equation 1.3, however the transmission coefficient is determined in the following way: If the electron's z directed energy, $W < V_{\max}$ then $D(W) = 0$ where as, for $W > V_{\max}, D(W) = 1$. This criteria can be used to easily obtain equation 1.15.

When there is an external electric field applied between the cathode and the anode, electron emission cannot be explain on the basis of the RLD alone. This is frequently called field enhanced thermionic emission and in this case the RLD equation is corrected for the Schottky effect. The lowering of the potential barrier at the surface of a metal due to presence of an electric field is known as the Schottky effect [10]. This effect is incorporated by adding image charges outside the metal surface. The "effective" work function is then reduced by an amount $\Delta\phi = \sqrt{\frac{e\mathbf{E}}{4\pi\epsilon_0}}$ and the current density is then given by

$$\mathbf{J} = A_G T^2 \exp\left[-\frac{\phi - \Delta\phi}{kT}\right] \tag{1.17}$$

However, even this correction is valid only for electric fields lower than 10^8 V/m. For higher electric fields, a combined thermal-field emission theory is more appropriate as this does not consider a simplistic transmission coefficient as in case of thermionic emission.

Thermal-Field Emission

The most prominant contribution to a combined theory of thermionic and field electron emission is probably the one given by Murphy and Good in 1956 [5]. They developed a set of equations for thermionic emission regime, field emission regime and an intermediate emission regime. The calculations were based on a general expression for emitted current as a function of temperature, field, and work function, in the form of a definite integral. This general equation is formed using Fermi-Dirac free electron distribution in the metal and classical image charge barrier at the surface.

The transmission coefficient, $D(W)$, is still considered to be 1 for $W > W_l$, where the limiting value, $W_l = -\frac{1}{2}\sqrt{2e^3\mathbf{E}}$. Although this is not accurate, it simplified calculations a lot and the results are relatively accurate for the range of applicability. The general emission current equation is then given by [5]

$$\mathbf{J}(\mathbf{E},T,\phi) = e\int_{-W_a}^{\infty} D(\mathbf{E},W)N(T,\phi,W)dW \tag{1.18}$$

$$= \frac{4\pi mkTe}{h^3}\int_{-W_a}^{W_l} \frac{\ln\{1+\exp[-(W+\phi)/kT]\}dW}{1+\exp[\frac{4}{3}\sqrt{2}(\mathbf{E}\hbar^4/m^2e^5)^{-\frac{1}{4}}y^{-\frac{3}{2}}v(y)]} + \frac{4\pi mkTe}{h^3}\int_{W_l}^{\infty}\ln\{1+\exp[-(W+\phi)/kT]\}dW \tag{1.19}$$

This equation (1.19) can be made to look better in terms of Hartree units.

The technique for evaluating the integrals in equation 1.19 is using different approximations depending on the conditions of temperature and field. Thus, for thermionic emission regime the conditions are given by

$$\ln\left[\frac{1-d}{d}\right] - \frac{1}{d(1-d)} > -\pi\mathbf{E}^{-\frac{3}{4}}(\phi - \mathbf{E}^{\frac{1}{2}}) \tag{1.20}$$

$$\ln\left[\frac{1-d}{d}\right] - \frac{1}{1-d} > -\pi\mathbf{E}^{-\frac{1}{8}} \tag{1.21}$$

$$\text{where,} \qquad d = \frac{\mathbf{E}^{\frac{3}{4}}}{\pi kT}$$

Now, the approximation used is the first term in an expansion of the logarithm above the Fermi energy and the first term in an expansion of the exponent in the denominator about the peak of the barrier. This leads to an integral which can be evaluated in terms of elementary functions. Without going into all the detailed step, which can be found in reference [5], the final expression for current density due to thermionic emission is given by

$$\mathbf{J} = \frac{1}{2}\left(\frac{kT}{\pi}\right)^2\left(\frac{\pi d}{\sin\pi d}\right)\exp\left[-\frac{\phi - \mathbf{E}^{\frac{1}{2}}}{kT}\right] \quad (\text{ A/m}^2) \tag{1.22}$$

This equation (1.22) can be seen to be similar to the RLD equation (1.15) apart from

the difference of the Hartree units used for defining energy in place SI units. Hartree unit is a unit of energy defined as $E_h = \hbar^2/m_e a_0^2$ where a_0 is the Bohr radius.

In parallel with the treatment of thermionic emission, the approximations used for the field emission regime is to use the first term in an expansion of the denominator-factor below the peak of the potential barrier and the first two terms in an expansion of the denominator-exponent about Fermi energy. The limits of this approximation and the applicability of the field emission equation are given by

$$\phi - \mathbf{E}^{\frac{1}{2}} > \frac{\mathbf{E}^{\frac{3}{4}}}{\pi} + \frac{kT}{1 - ckT} \tag{1.23}$$

$$1 - ckT > (2f)^{\frac{1}{2}} kT \tag{1.24}$$

$$\text{where,} \quad c = 2\sqrt{2}\mathbf{E}^{-1}\phi^{\frac{1}{2}} t(y)$$

$$\text{and} \quad f = \frac{1}{2}\sqrt{2}\mathbf{E}^{-1}\phi^{\frac{3}{2}}(\phi^2 - \mathbf{E})^{-1} v(y)$$

Then, using the above mentioned approximations the current density in the field emission regime is given by

$$\mathbf{J} = \frac{\mathbf{E}^2}{16\pi^2\phi t^2(y)} \left(\frac{\pi ckT}{\sin \pi ckT}\right) \exp\left[-\frac{4\sqrt{2}\phi^{\frac{3}{2}} v(y)}{3\mathbf{E}}\right] \tag{1.25}$$

Again, it can be noticed that this equation in the limit for low temperature is similar to (besides the Hartree units) F-N equation (1.12).

In the intermediate emission regime, which cannot be modeled by either pure field emission or pure thermionic emission, a saddle point approximation is used by Murphy and Good. The conditions of this approximation are

$$\text{first} \qquad \left(-\frac{\mathbf{E}^{\frac{1}{2}}}{\eta}\right)^{-1} > 1 + \frac{\mathbf{E}^{\frac{1}{4}} d}{\pi(d-1)} \tag{1.26}$$

$$\text{where,} \qquad d = 2\sqrt{2} t_\eta \pi^{-1} \left(-\frac{\mathbf{E}^{\frac{1}{2}}}{\eta}\right)^{\frac{1}{2}},$$

$$t_\eta = t\left(-\frac{\mathbf{E}^{\frac{1}{2}}}{\eta}\right),$$

$$\eta = -\frac{\mathbf{E}^2}{8(kT)^2} t_\eta^2 \qquad \text{and}$$

$$\text{second} \qquad -\frac{\mathbf{E}^2}{8(kT)^2 t_\eta} > -\phi + \frac{kT}{1 - \mathbf{E}(2\sqrt{2}\phi^{\frac{1}{2}} kT t(y))^{-1}} \tag{1.27}$$

The final expression for emission current density in the intermediate regime is then given by

$$\mathbf{J} = \frac{\mathbf{E}}{2\pi}\left(\frac{kTt_\eta}{2\pi}\right)^{\frac{1}{2}} \exp\left[-\frac{\phi}{kT} + \frac{\mathbf{E}^2\Theta}{24(kT)^3}\right] \tag{1.28}$$

$$\text{where} \qquad \Theta = \frac{3}{t_\eta^2} - \frac{2v(y)}{t_\eta^3}$$

Thus, the set of equations 1.22, 1.25 and 1.28 together describe combined thermal-field emission of electrons and are frequently called the Murphy-Good (M-G) equations. The bounding regions of validity of these equations is shown in figure 1.2. Recently, Jensen has published methods to combine thermal and field emission regimes for better accuracy and more range of validity using a method to find best approximated expansion point numerically and then use analytical approximation methods at that point to get the unified solution [2] [11].

1.1.3 Transfer Matrix Method (TMM) Model

In the previous sections we have seen electron emission theories that are analytical. The current density equation is calculated analytically by making certain assumptions depending on the potential barrier, temperature or electric field and so forth.

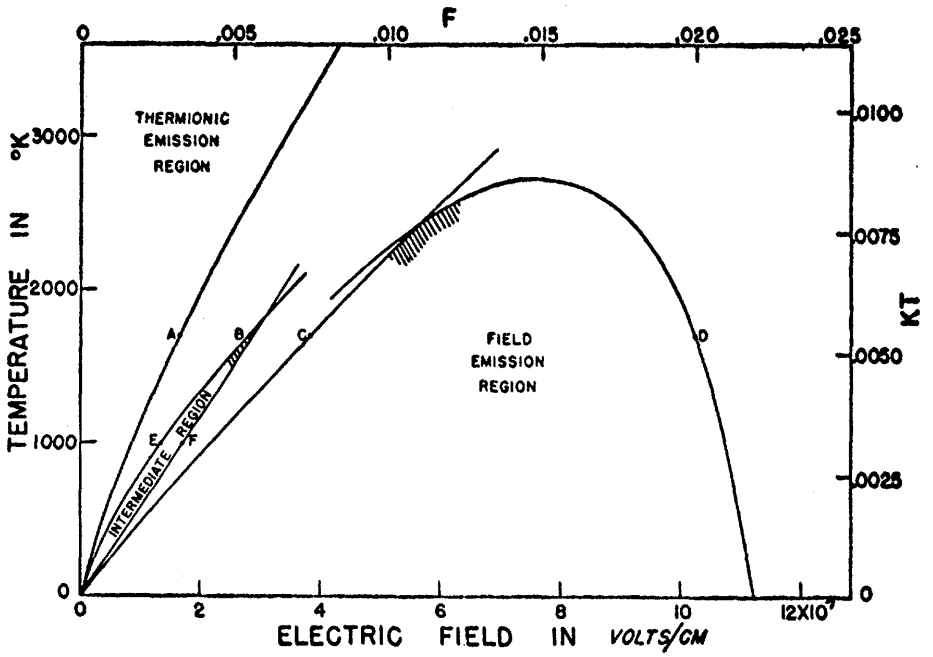

Figure 1.2: Plot showing bounds of validity of Murphy-Good equations showing thermionic, field and intermediate emission regimes [5].

Hence for the analytical solutions, ensuring that conditions for validity are satisfied is an important check before their use. There are other models for field emission as well as combined thermal-field emission that use numerical methods to solve intractable equations, instead of using approximations. I will be describing a Transfer Matrix Method (TMM) model that X. He developed in our lab [12], which numerically solves the Schrödinger's equation for a given potential barrier by TMM to get the transmission coefficient and calculates emission current density at any given temperature by numerically integrating equation 1.10.

The TMM model, like the above theories, assumes a Sommerfeld free electron model supply function, for which the Fermi-Dirac distribution applies. The potential barrier includes the image charge potential term. This potential barrier as shown in figure 1.1 is divided into many narrow rectangles. The number of divisions of the potential barrier needs to be high enough for the TMM to converge and give result

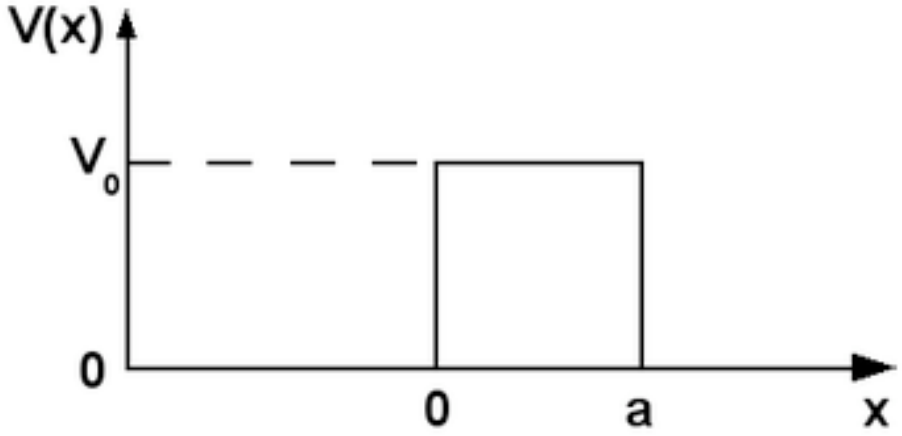

Figure 1.3: A finite rectangular potential barrier

within acceptable error value. This number depends on the surface electric field, lower fields required higher number of rectangles since the barrier is thicker [13].

For a single rectangular barrier shown in figure 1.3 the transfer matrix of transmission, $\mathbf{T}$ can be found multiplying the transfer matrix of transmission from region 1 (left of $x = 0$) to region 2 (right of $x = 0$), $\mathbf{T}^{12}$, and the transfer matrix of transmission from region 2 to region 3 (right of $x = a$), $\mathbf{T}^{23}$[14]. Thus,

$$\mathbf{T} = \mathbf{T}^{12}\mathbf{T}^{23}. \tag{1.29}$$

$$\text{and,} \quad \mathbf{T} = \begin{bmatrix} T_{11} & T_{12} \\ T_{21} & T_{22} \end{bmatrix} \tag{1.30}$$

Then the transmission probability, t and transmission coefficient, T are

$$\begin{aligned} t &= \frac{T_{11}T_{22} - T_{12}T_{21}}{T_{22}} \\ &= \frac{2k_1k_2e^{-ik_1a}}{2k_1k_2\cos k_2a - i(k_1^2 + k_2^2)\sin k_2a} \end{aligned} \tag{1.31}$$

$$\text{and,} \quad T = t^*t = |t|^2 = \frac{4k_1^2k_2^2}{4k_1^2k_2^2 + (k_1^2 - k_2^2)\sin k_2a} \tag{1.32}$$

here k_1 and k_2 are the wave numbers of the Schödinger's equation in region 1 and 2

respectively.

In this manner, each rectangular barrier is multiplied by its next neighboring rectangular barrier, to eventually cascade all the segments of the arbitrary 1-D potential and evaluate a total transfer matrix and thus, a total transmission coefficient, $D(W)$. Once $D(W)$ is calculated, the current density, $\mathbf{J}$, is calculated by numerically integrating the equation 1.10. The TMM model shows good agreement with the combined set of M-G equations [13].

1.2 Field Emission Applications

Field Emission has a number of applications mainly due to its advantages as an electron source over conventional thermionic and photoelectron sources. The main advantages of field emission are:

- Field emission has a higher efficiency of emission than any other emission process since there is no dissipation of energy in tunneling through a barrier and electron transport in vacuum.

- High temperatures are not required as the electron kinetic energy need not be higher than the potential barrier. This makes field emission perfectly suited for applications that require lower temperature.

- Since electron transport in vacuum is without resistance, there is a virtual lack of inertia in the field emission process. This can permit its use in fast or high frequency applications.

- Field emission can be capable of giving very high current densities and high power capabilities.

- The electron emitter or cathode can be used for a longer time since it runs in vacuum and is not required to operate at a high temperature. Hence field emission cathodes inherently have higher radiation tolerance and heat resistance.

- The electrons emitted via field emission process have a small spread in energy, which is very important for applications of electron microscopy and spectroscopy.

With so many advantages it is not surprising that field emission has a number of applications. It is replacing thermionic emitters as electron sources at the same time it has found various new applications in future products. A few main applications are described below in this section.

High Power Microwaves

A classic application of electron beams is generation of coherent electromagnetic radiation in the "microwave" frequency range (300 MHz to 300 GHz). The idea of field emission cathodes as replacements for Thermionic emitters started around late 1950's and early 1960's [15]. The performance of any microwave device depends critically on the electron beam that drives the device, and this is where the advantages of field emission as a source of electron beam gives it an advantage over other electron emission mechanisms. The principle of operation of these devices based on the transfer of energy from an electron beam to an electromagnetic field. Three fundamental radiation mechanisms are involved here known as Cherenkov radiation, transition radiation and Bremsstrahlung radiation. Since this thesis is related to field emission and not microwave devices, details of their working is not provided here, but can be found in reference [16]. Field emitter arrays are replacing thermionic emitters as electron beam sources for these high power microwave devices because of their superior properties. Field emission can produce electron beams that are of better "quality". By "quality"

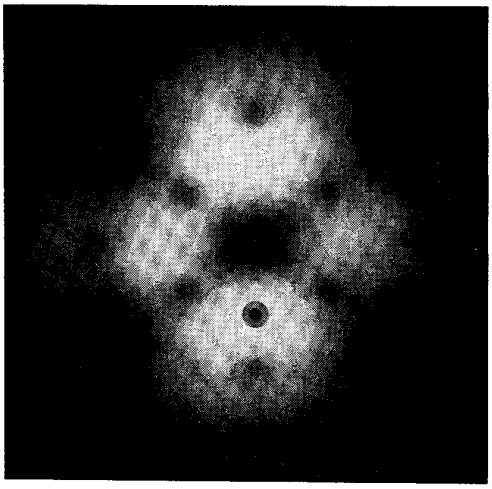

Figure 1.4: A typical FEM image of a clean single crystal Tungsten showing the crystal face (011) in the center and (012) on the sides.[17]

one means the spatial, energy, and momentum spread in the electron beam.

Electron Spectroscopy and Microscopy

Field electron emission can be used to study surfaces. The electrons emission from a surface is a function of the local work function of that surface. It is well known that different crystal faces have a different work function due to a difference in spatial distribution of electrons. As a result emission current densities from different faces is different for the same applied voltage. This allows mapping electron emission to create magnified surface images by a technique called Field Emission Microscopy (FEM), due to E. W. Muller. FEM also allows measurement of the work function of these different crystal faces [17]. Figure 1.4 shows a FEM image of a clean Tungsten surface, from which it is possible to calculate the crystal face work function. In FEM, the information about the surface contained in the electron energy distribution is forfeited in order to retain the spatial information for microscopy. However, if electrons from only a small area of the surface are collected and energy analyzed, then its called

Field Emission Spectroscopy (FES). FEM and FES together are very important tools to study and characterize surfaces and surface phenomenon.

Flat Panel Display technology

Small field emitters can be put in an array to make a flat panel display, called Field Emission Display (FED). Thus, a FED is a vacuum device in which millions of microscopic field emitters emit electrons that travel to a patterned phosphor screen. Due to the need for small anode-cathode spacing to get a large field these displays are inherently thin and low weight. The thickness of a FED without driver electronics is typically 5-7 mm [18]. This FED has been shown to have superior properties as compared to other flat panel display technologies such as LCDs and PDPs and are considered very attractive replacements for LCDs and PDPs, however a lot still remains to get this idea from research to the point of being a manufacturable technology.

Electric Propulsion

The need for low power (< 100 W) and energy efficient electric propulsion systems for satellites and spacecrafts may benefit from electron sources which use field emitters to ionize the propellant and neutralize the ion beam for Hall thrusters. Recent advances [19] have been made in terms of lifetime, low power consumption and lower size for these field emission neutralized thrusters and they look like a promising technology for space propulsion.

A number other technological contexts of field emission are important to be mentioned. For instance, field emission is the internal electron transfer mechanism in some type of solid state devices. The avoidance of field emission, and hence vacuum breakdown is important in many contexts, notably in high-voltage particle accelera-

tors. Field emission arrays may be able to meet the needs of radar and communication applications that require high current densities as well as fast turn on and turn off times.

Chapter 2

The Experimental System

Experiments on field electron emission were carried out in the Vacuum Electronics lab with the modified Madison Cathode Experiment (MACX) setup. This chapter describes the modified MACX system in detail. The Ultra High Vacuum (UHV) system, the anode-cathode (A-K) system, the power and high voltage (HV) pulsing setup as well as the measurement setup are described. This chapter also describes the design of the Copper Knife Edge (CKE) cathodes used in the experiments. Some modifications were done to the basic structure of the cathode subsequently, like chemical etching and thin film deposition, which will be discussed in later chapters.

2.1 MACX Description

MACX setup consists of the UHV system, capable of a base pressure of 10^{-10} Torr, and the A-K system, capable of local micro current measurement through a aperture and Faraday cup setup. This section describes MACX with its component systems in detail.

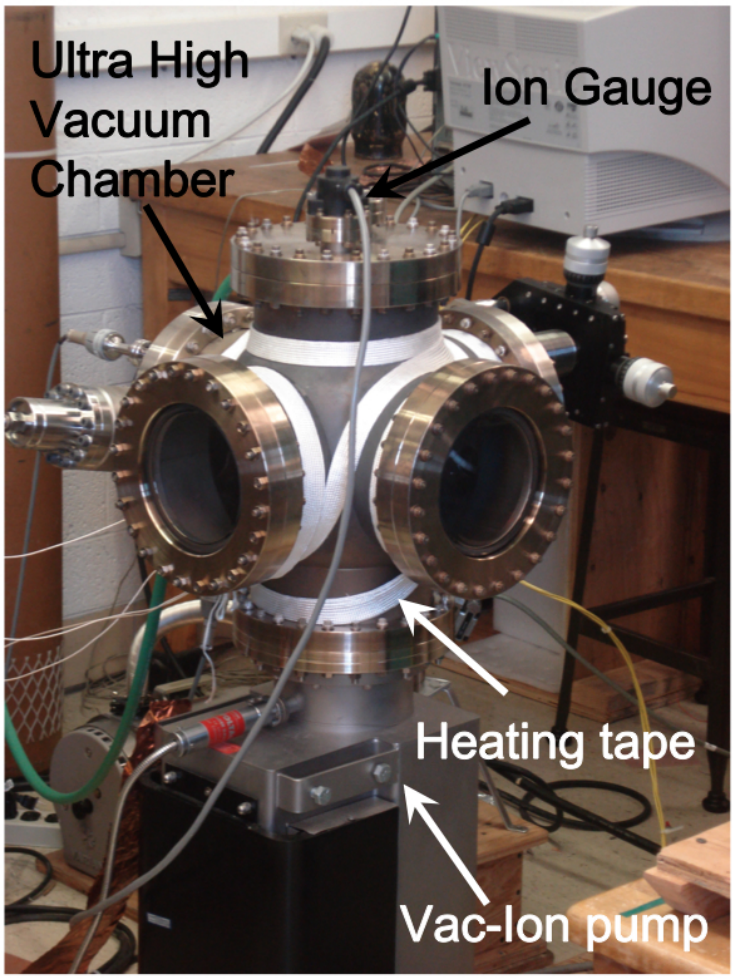

Figure 2.1: A picture of the UHV system showing some of its components

2.1.1 UHV system

The UHV system consists of a six-way UHV chamber, with three stages of pumping and three pressure gauges. A picture of the UHV system is shown in figure 2.1. The first pump is a Varian scroll pump which can lower pressure upto 10^{-1} Torr. The second stage is a Varian Turbo pump that runs with $\sim 55,000$ rpm and can lower the pressure upto 10^{-7} Torr. The third and final pumping stage is a 250 L/s Vac-Ion pump and which can reduce the pressure down to 10^{-10} Torr. The turbo pump is connected through an all-metal bakeable right angle valve to isolate the system after

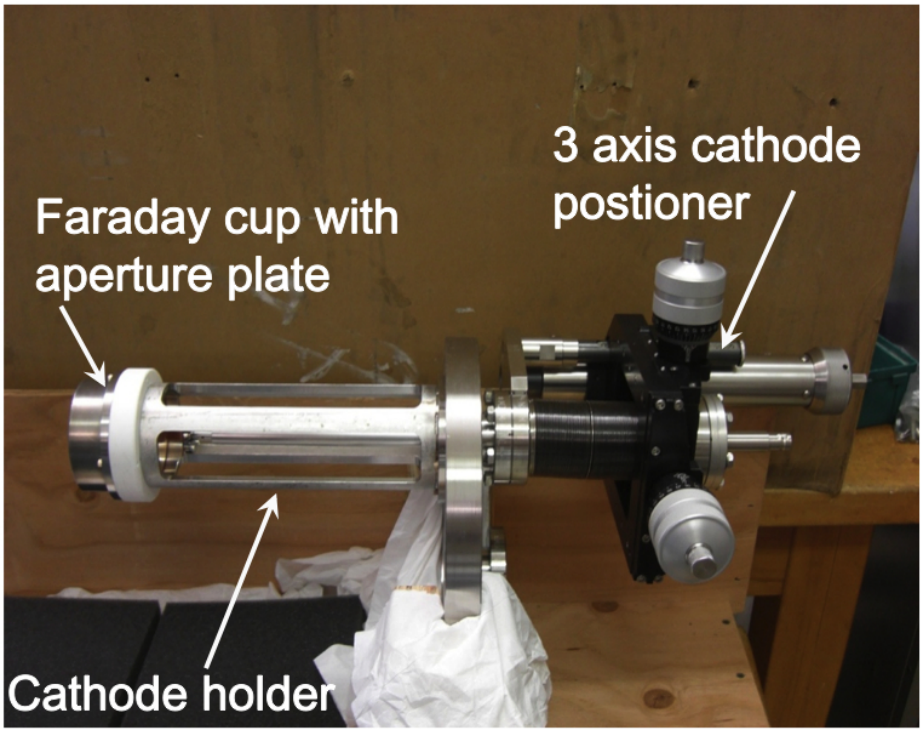

Figure 2.2: A picture of the A-K system showing some of its components

it has reached a pressure of $\sim 10^{-7}$ Torr. After this stage the whole system is baked using two heating tapes upto 350 ℃, for several days to eliminate moisture from the surface of the chamber. By the end of baking with the Ion pump running a pressure of 10^{-10} Torr can be achieved. The UHV system also has two ConvecTorr pressure gauges and one Ion gauge to measure the pressure during each stage at different locations in the system. A nitrogen induction system is also connected to the UHV chamber and used when the chamber requires to be opened for replacing a cathode. With such a high vacuum, most of the interference from contaminants is eliminated in addition to plasma formation due to field emission and hence the experiments can focus on the physics of field emission.

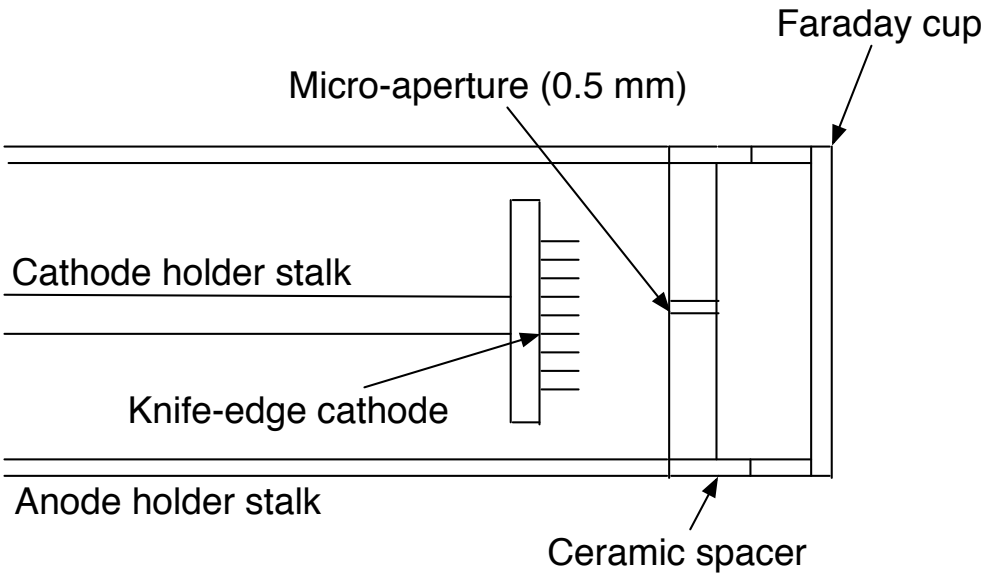

Figure 2.3: A schematic of the micro-aperture anode, faraday cup and the cathode holder arrangement

2.1.2 A-K system

The A-K system consists of a cathode holder and the anode assembly. The steel tube cathode holder is connected SHV20 coaxial feedthrough for electrical supply and also connected to a 3-axis positioner through bellows, which can be used to move the cathode with respect to the anode assembly. The anode assembly consists of a flat copper plate anode with a micro aperture of 0.5 mm diameter and a Faraday cup back anode to collect electrons escaping from the micro aperture. This assembly is also connected on the outside through two SHV20 coaxial feedthroughs for measurement of current. The whole system is bakeable upto 350℃, which allows experiments to be done at elevated temperatures. The figure 2.2 shows a picture of the A-K system and figure 2.3 shows a schematic drawing of the micro-aperture anode, faraday cup and the cathode holder.

Using the 3-axis positioner the cathode can be positioned relative to the aperture

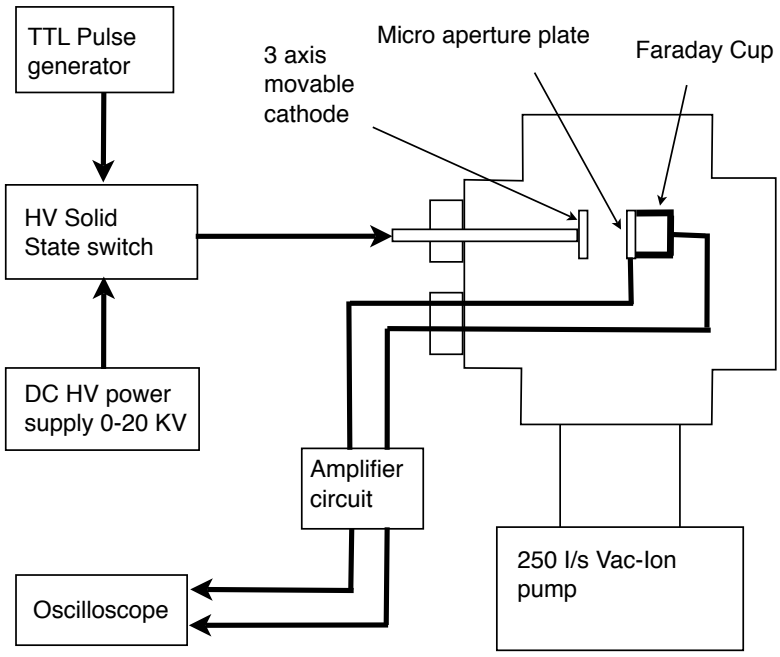

Figure 2.4: A schematic block diagram depicting the MACX system along with the pulsing and measurement setup

in the plate anode and lateral as well as transverse scans over the cathode surface can be done collecting local emission current from the aperture by the Faraday cup. The positioner has a resolution of 0.001 inches in the x-y axes, which allows emission current mapping over the surface of the cathode. The z-axis positioner also has a resolution of 0.001 inches by the provision of an external dial. This dial can be reset to zero upon getting contact between the anode plate and the cathode. Thus by using this external dial, the error due to thermal expansion at high temperatures can be eliminated.

2.1.3 Pulsing & Measurement Setup

The Pulsing setup consists of HV Glassman DC supply working with a signal generator, controlling a HV DEI solid state switch. This supply can provide 0 to 10 kV

negative pulses of duration 1 μs to 5 s, with pulse rise times less than 60 ns. It can provide upto 300 mA of current and is suitable for field emission experiments. The measurement setup consists of coaxial cables coming form the feedthroughs of the UHV chamber going to a wide range 3-stage cascaded low noise amplifier to a LeCroy WaveRunner measurement oscilloscope, where the data is recorded. A schematic block diagram depicting the system is shown in figure 2.4

The primary challenges in measurement of emission current was the wide dynamic range (from a few nA to a few hundred mA), very high transient current spikes with relatively very low steady-state current levels and the overall noise reduction for enabling measurement of a few nA of current. To overcome these problems we designed a 3-stage cascaded low noise amplifier with a 1 MΩ resistor placed in series with the measurement loop (to reduce transient current spikes). Figure 2.5 shows a circuit diagram of one stage of the amplifier. After each stage of amplification we inserted parallel forward/reverse Schottky diodes as voltage/current limiters to further reduce the transients being amplified along with measurement currents. To reduce noise, each stage of the amplifier is connected with a filtering feedback circuit. These RC filters increase the signal-to-noise ratio. With this amplifier it is possible to get a gain in three steps, first stage gives a gain of 11, along with second the gain becomes, 121, and with all the three stages connected a gain of 1331 can be obtained. All cables used are coaxial for excellent shielding and ground connectors are very wide copper strips. This setup permits detection and measurement of emission currents down to ~ 2 nA.

2.2 CKE Cathode

The CKE cathode is fabricated from a copper alloy by wire Electro-Discharge Machining (EDM). The raised ridges or knife edges are about 130 μm wide and about

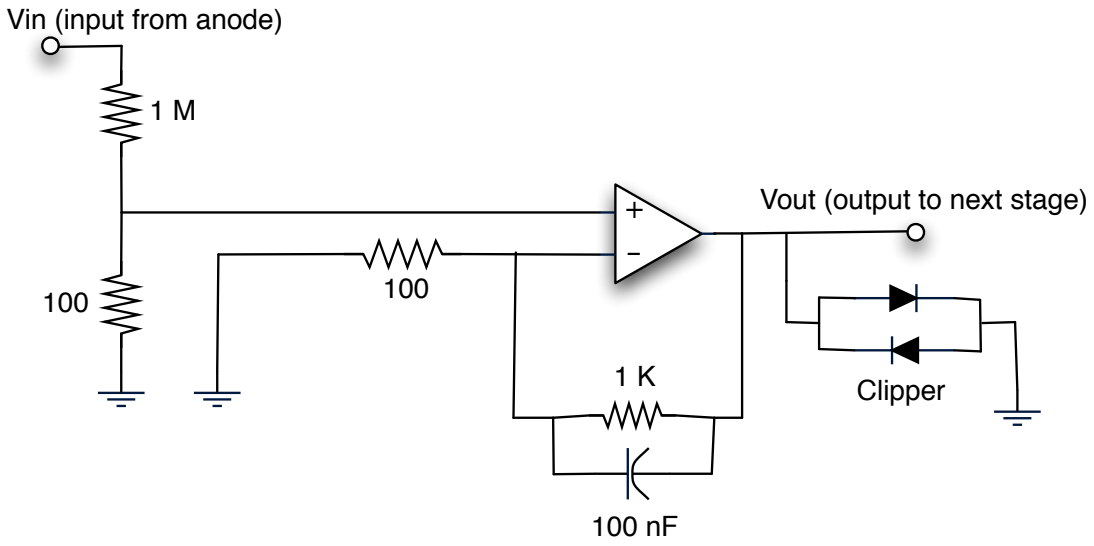

Figure 2.5: A circuit diagram of one stage of the amplifier

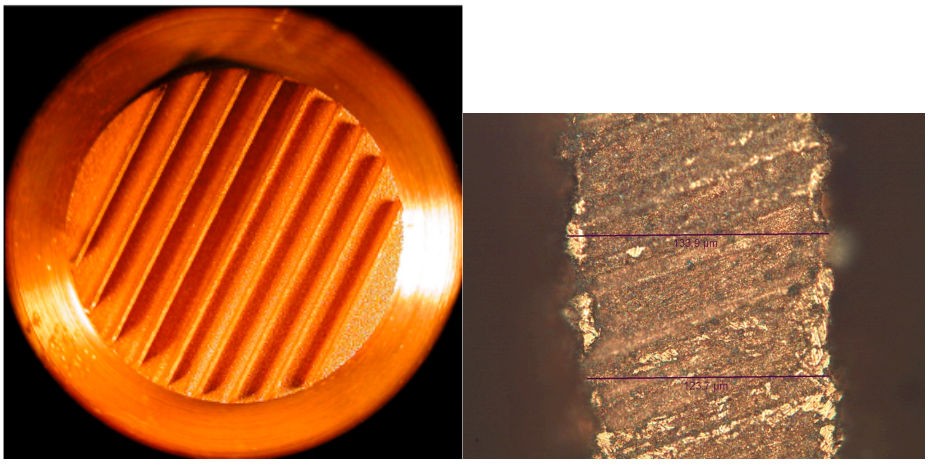

(a) CKE cathode **(b)** Close up of a knife edge

Figure 2.6: Pictures of CKE cathode (a) showing its geometry and (b) close up of knife edge showing surface morphology of emission area

1.5 mm high. Figure 2.6 shows a picture of the cathode and a close up of its knife edge structures. The area of the cathode, A, is calculated as the area on top of the knife edges and is about 9 mm^2. This is the cathode that was used for the preliminary experiments. After analyzing the results of emission from this cathode, we decided to etch the knife edges chemically to make then thinner and as a result increase their aspect ratio. A higher aspect ratio results in a higher field enhancement factor, β [20] and as a result emits higher emission current density. And subsequently, we decided to deposit a low work function material thin film on these cathodes to get higher current density. These cathodes will be discussed in later chapters along with the motivation for fabricating them and their results.

Chapter 3

Experiments with CKE cathode

Having described the background theory and the experimental system, we can now proceed to the experiments done with the CKE cathode. This chapter describes those experiments, the results and analysis. The first step with this new modified MACX system was to check using a cathode similar to one used by X. He [12]. This cathode is called the CKE4 cathode as it was the fourth cathode from its batch. The figure 2.6 shows pictures of CKE4 cathode.

3.1 Preliminary Experiments on CKE4

The preliminary experiments consisted of simple emission current measurement experiment from the surface of the whole cathode as was done by X. He earlier during this project. The intention was to check whether the emission currents would be high enough to enable measurement of local emission currents using the micro-aperture and Faraday cup arrangement. CKE4 cathode was use for these experiments as described below.

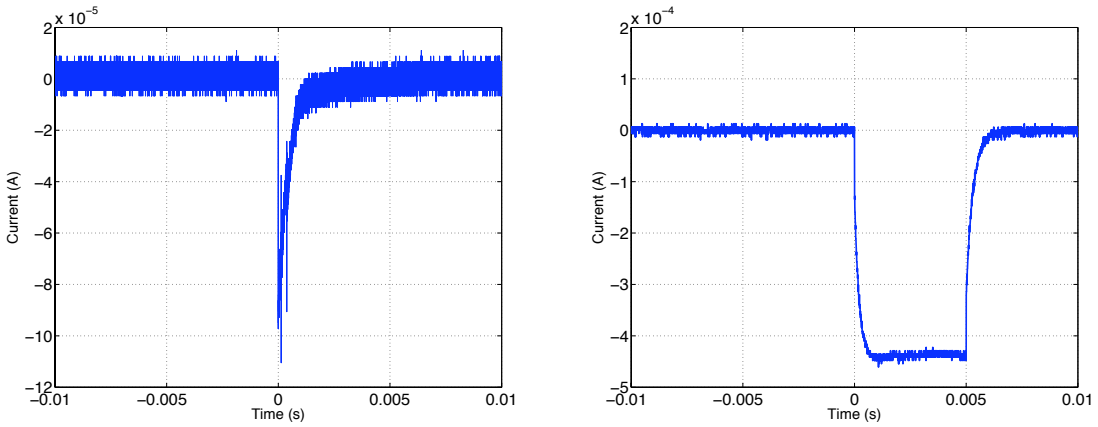

(a) Before Conditioning

(b) After Conditioning

Figure 3.1: Showing the effect of conditioning on emission current from CKE4 cathode

3.1.1 Experiment

The CKE4 cathode (shown in figure 2.6) was mounted in the cathode holder and the process of vacuum pump down was initiated. This process takes about 2-3 days. The base pressure achieved before these experiments was $\sim 6 \times 10^{-10}$ Torr. This base pressure is sufficient for field emission experiments as arcing and plasma formation due to explosive emission is eliminated. Before the actual experiment and recording of data, the cathode needs to be conditioned. Conditioning is a process of applying about $10,000$ or more high voltage pulses (> 7 kV) to the cathode at a high frequency to dislodge loose contaminants from the surface and make the emission from the cathode stable. Without conditioning reliable data cannot be obtained. Conditioning was started at 7 kV and the voltage was slowly increased up to 10 kV. The emission waveform after conditioning, figure 3.1(a), can be seen to be stable and flat as opposed to before conditioning, figure 3.1(b).

Once a stable emission current is observed from the cathode, the experiment can

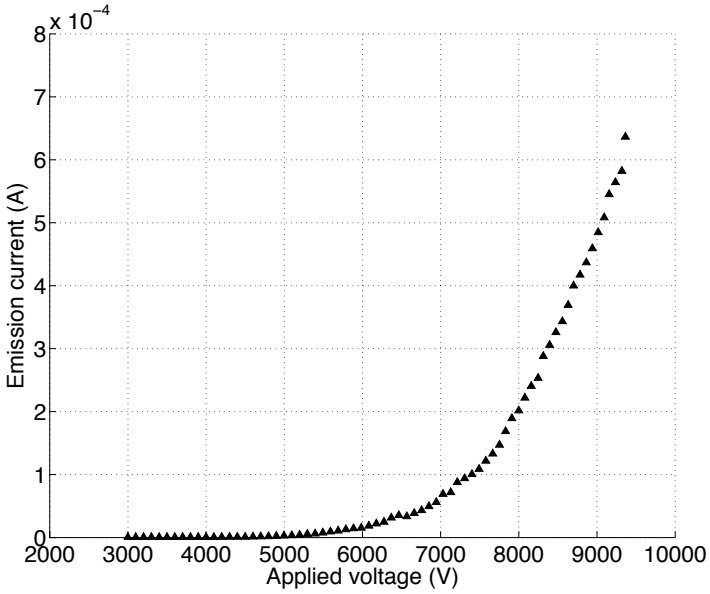

Figure 3.2: Plot of emission current versus the applied voltage for CKE4 cathode at room temperature

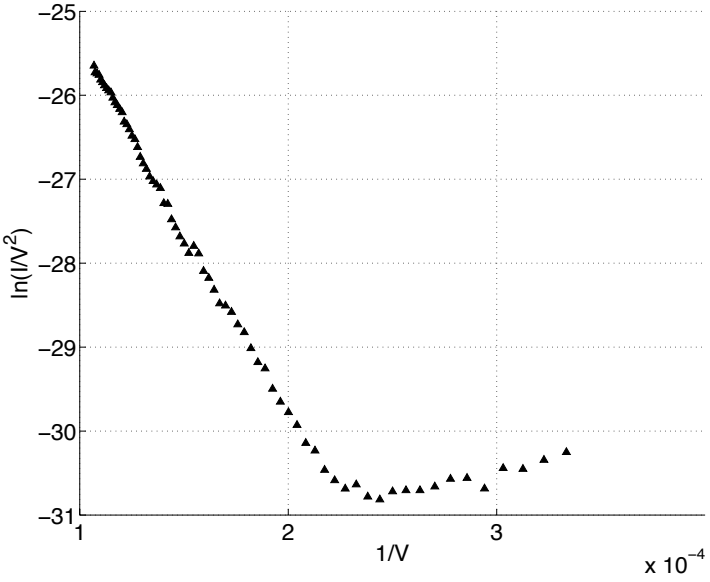

Figure 3.3: Plot in Fowler Nordheim coordinates for CKE4 at room temperature

be started. For this experiment, the pulse width was kept at 5 ms and each data point was averaged over ~ 100 shots. The first experiment was done at room temperature with decreasing voltage, starting from 10 kV and going down up to 3 kV and recording data in steps of 0.1 kV. The corresponding plots of emission current versus applied voltage and F-N plots are shown in figures 3.2 and 3.3.

Figure 3.2 shows that the emission current increases exponentially with applied voltage, which is seen in case of field emission. Further proof of this being field emission current comes from figure 3.3 which shows the emission current and voltage plotted in the F-N coordinates given by $\ln I/V^2$ for the y-axis and $1/V$ for the x-axis. A straight line in these coordinates signifies the emission current to be related to voltage by F-N type equations [21]. However in figure 3.3, the straight line curve reaches a minimum and changes slope. This low Electric field emission current is accounted for by thermal-field emission [22] [23] [24].

3.1.2 Results & Analysis

The analysis of experimental data was done considering the low electric field emission to be due to thermal effects. Using thermal-field emission data, it is possible to independently extract both the work function ϕ, and the field enhancement factor β. Different techniques are utilized to do this as described in references [22] and [24]. The procedure used here was to extract the work function from the low electric field region using the RLD equation corrected for the Schottky effect also known as field enhanced thermionic emission given in equation 1.17. This equation is plotted for room temperature for different ϕ to match the experimental data. It is seen from figure 3.4 that $\phi = 2.96$ eV gives the best match to the experimental results. Then using this value of ϕ in the high electric field region it is possible to extract β using the slope of the F-N plot.

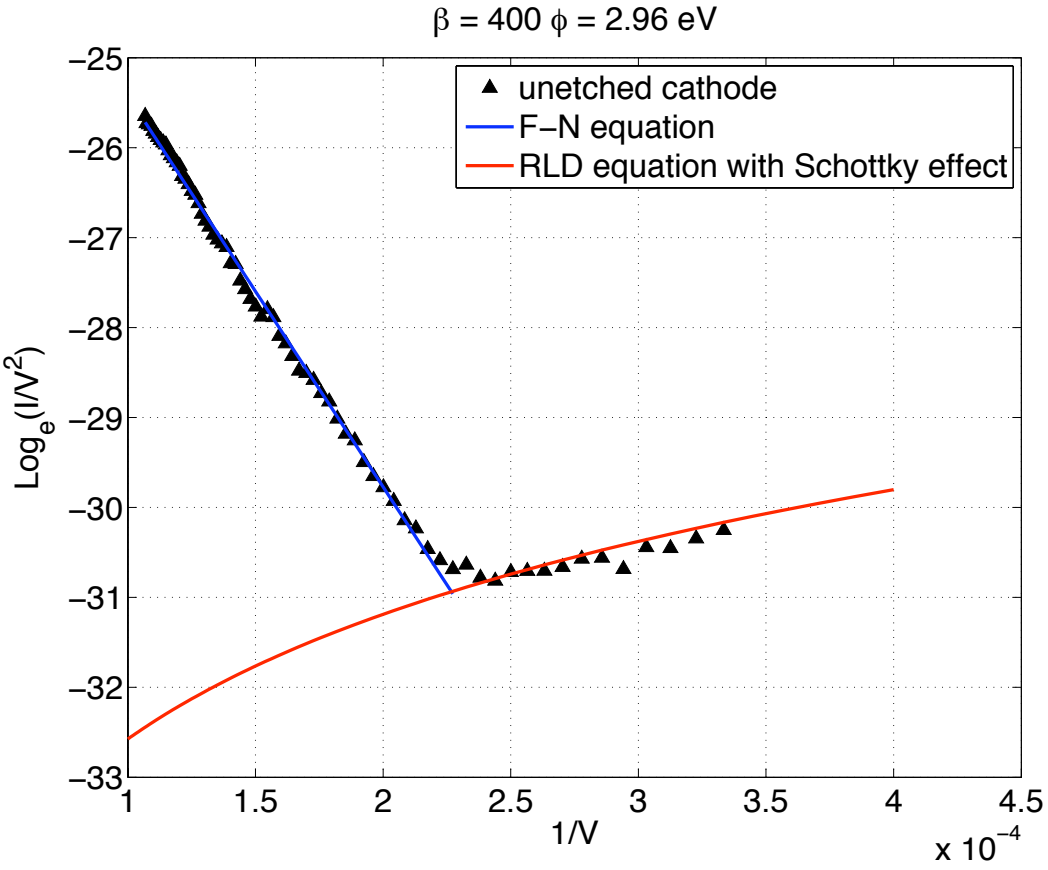

Figure 3.4: Extracting the work function, ϕ from the low field region using RLD equation modified for Schottky effect (resulting in $\phi = 2.96$ eV) and field enhancement factor, β from the high field F-N plot slope for CKE4 (resulting in $\beta \approx 400$)

In equation 1.12, putting $\mathbf{J} = I/A_e$, where $A_e = 9 \times 10^{-6}$ m^2 is the emission area taken to be equal to the area on top of the knife edges, $\mathbf{E} = \beta V/d$, where V is the applied voltage and d is the anode cathode distance and taking the natural logarithm on both sides, we get,

$$\ln \frac{I}{V^2} = \ln \frac{A_e A \beta^2}{d^2 \phi t^2(y)} - \frac{B v(y) \phi^{\frac{3}{2}} d}{\beta} \frac{1}{V} \tag{3.1}$$

From the above equation 3.1 it can be seen that the slope, S and the intercept, $\ln R$ of the F-N plot is given by,

$$S = -\frac{B v(y) \phi^{\frac{3}{2}} d}{\beta} \tag{3.2}$$

$$R = \frac{A_e A \beta^2}{d^2 \phi t^2(y)} \tag{3.3}$$

For the electric fields in question it is accurate enough to assume that the functions $v(y)$ and $t(y)$ as equal to unity. The tabulation of these functions can be found in many papers for example reference [25]. Using this value for the slope (equation 3.2), β can be readily calculated from the experimental data and the resulting $\beta = 400$.

Having extracted ϕ and β, these parameters could now be used to extract the emitting area. Forbes theory for determination of emitting area from F-N plots [26] was used for this. In this method, the fitted straight line in the empirical local-field based F-N plot is represented by

$$\ln\{I/V^2\} = \ln R + S/V \equiv \ln\{r R^{\mathrm{el}}\} + s S^{\mathrm{el}}/V, \tag{3.4}$$

where the quantities $r(\equiv R/R^{\mathrm{el}})$ and $s(\equiv S/S^{\mathrm{el}})$ are factors that represent corrections to the predictions of elementary F-N theory and are termed, the intercept correction factor and slope correction factor, respectively. Then to interpret empirical results in terms of the theory, the relationship between r, s, y, $t(y)$ and $v(y)$ is determined and

used to find the emitting area. These relations are given below [25]:

$$y = cF^{1/2}/\phi; \tag{3.5}$$

$$v(y) = 1 - y^2 + y^2 \ln y/3; \tag{3.6}$$

$$s(y) = 1 - y^2/6; \tag{3.7}$$

$$t(y) = 1 + (y^2 - y^2 \ln y)/9; \tag{3.8}$$

$$u(y) = 5/6 - \ln y/3; \tag{3.9}$$

$$r(y) = t(y) \exp[gu(y)\phi^{-1/2}] \tag{3.10}$$

where $c \equiv (e^3/4\pi\epsilon_0)^{1/2} = 3.794687\times10^{-5}$ eV m$^{1/2}$/V$^{1/2}$ and $g \equiv bc^2 = 9.836$ eV$^{1/2}$. The parameter β can be eliminated by using the combination RS^2 and so from the definition of r and s, the emitting area is written as

$$A = \frac{RS^2}{C_2\Gamma}, \tag{3.11}$$

where C_2 is a universal constant given by $ab^2 = 7.192489 \times 10^{13}$ A/m^2 eV^2 and Γ is a new function called the emission area extraction function and is given by $\Gamma = rs^2\phi^2$. Thus, by using this method we were able to extract the emission area for CKE4 using the independently calculated β and ϕ values. The variation of emission area for CKE4 is shown in figure 3.5 and the average emitting area is found to be 6.66×10^{-7} m^2 which is a reasonable value considering the area on the top of the knife edges to be equal to 9×10^{-6} m^2.

The next step was to perform local emission current measurements. However, the emission current level was very low, emission current profile scans over the surface using the aperture and Faraday cup setup described in chapter 2 on page 20 were not possible to detect currents above noise levels. Hence, to get higher emission current, the CKE4 cathode knife edges were etched to make them thinner, resulting in higher field enhancement and hence higher emission current density.

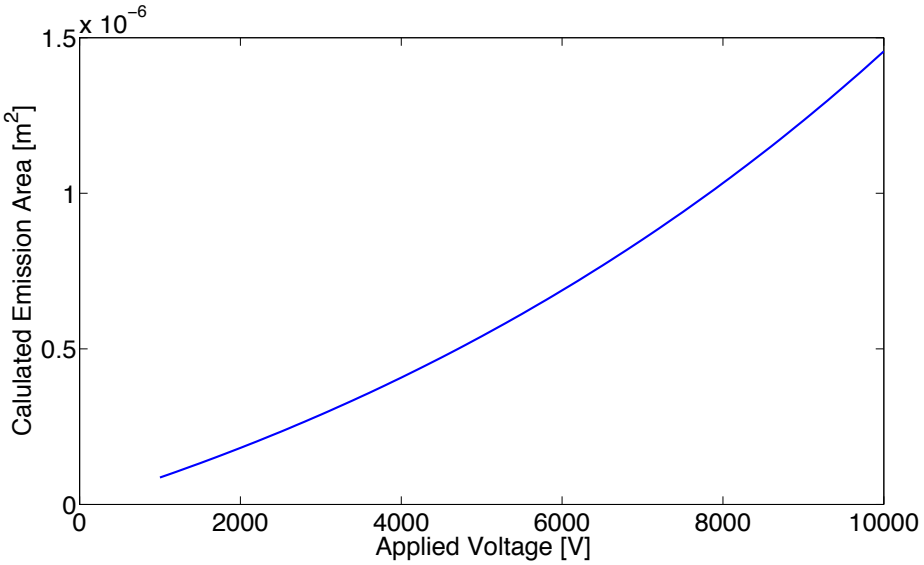

Figure 3.5: Variation of emitting area as calculated using Forbes' method for CKE4 cathode.

3.2 Experiments on etched CKE4

This section describes the etching process as well as the experiments on the etched CKE4 cathode. The etched cathode produced higher current densities enabling local current measurements, which are also described in this section.

3.2.1 Etching

The CKE4 cathode was subsequently chemically etched using a solution of Cupric Chloride ($CuCl_3$), to make the knife edges or ridges narrower and create higher field enhancement to get more current density. $CuCl_2$ was chosen as the etchant after reviewing its superior qualities over other common etchants like Alkaline etchants, Hydrogen Peroxide - Sulphuric acid ($H_2O_2 - H_2SO_4$), Chromic - Sulphuric acid ($CrO_3 - H_2SO_4$), Ferric Chloride ($FeCl_3$) and various others [27]. The chemical reac-

tion that results in etching of copper is as shown below:

$$CuCl_2 + Cu \rightarrow 2CuCl \tag{3.12}$$

A one molar $CuCl_2$ solution was diluted in equal amount of water to get a 0.5M solution. The copper CKE4 cathode was lowered in the solution which was kept in a glass beaker. The solution in the beaker was agitated using a chemical mixer at the same time the beaker was heated to a temperature of 50 ℃, to facilitate etching. After the process of etching the copper cathode was cleaned in an ethanol bath. The cathode was also baked to a temperature of 300 ℃, during the process of getting vacuum in the MACX system. The baking should remove the water vapor and other loose contaminants from the surface giving a clean copper surface.

After etching the dimensions of CKE4 cathode were measured and it was seen that the knife edge thickness was reduced from $\sim$ 130 μm to 5–30 μm. In addition to narrowing of the knife edges, it was seen that the etching process has made them non-uniform in thickness along their length. Figure 3.6 shows pictures of the etched CKE4 cathode.

3.2.2 Experiment: Total emission current

The etched CKE4 cathode was put through the same process as described in the first sub-section of this chapter. After achieving a good UHV, the cathode was conditioned to get stable emission current. The first experiment again consists of measuring the total emission current as a function of applied voltage. It was observed that the etched CKE4 cathode emits considerably higher current (an order of magnitude higher). Figure 3.7 shows the plot of emission current as a function of voltage across anode and cathode. This was reassuring as we expected that the larger aspect ratio will produce a higher β and result in higher emission currents. What was however not expected, is seen from the F-N plots in figure 3.8. The etched cathode does not show

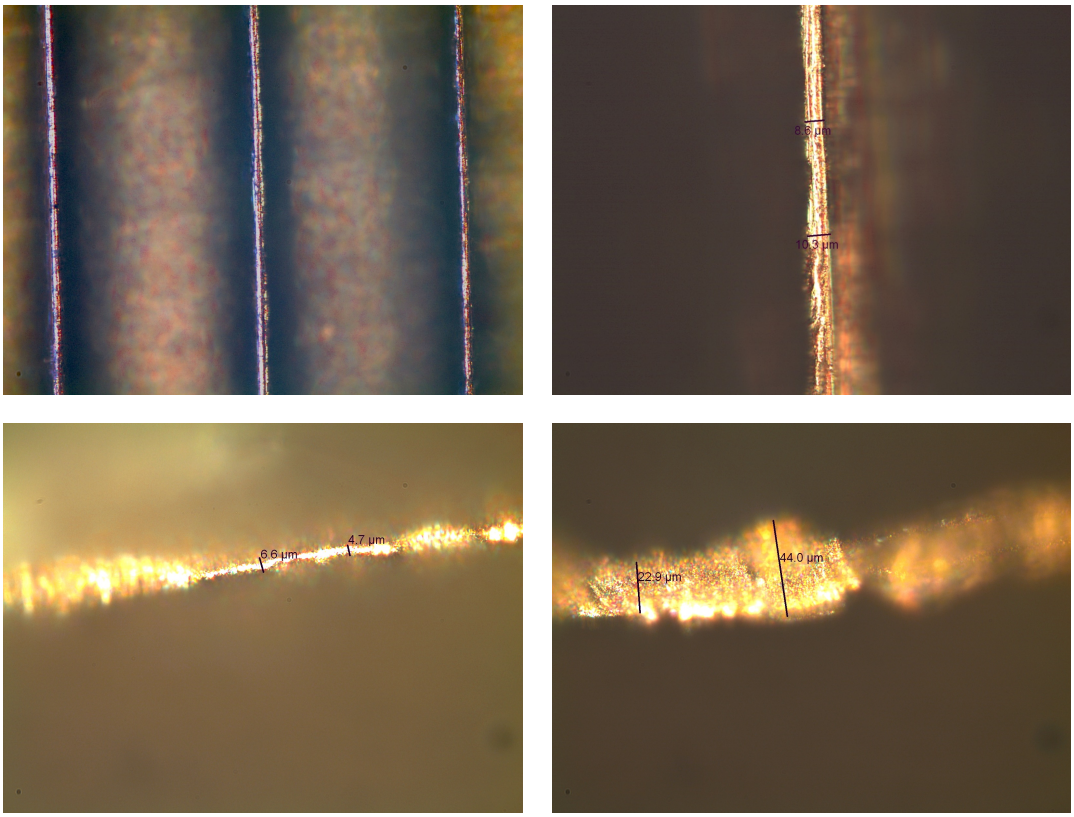

Figure 3.6: Pictures of CKE4 after etching, showing reduction in knife edge thickness and non-uniformity along knife edge length under 10x magnification

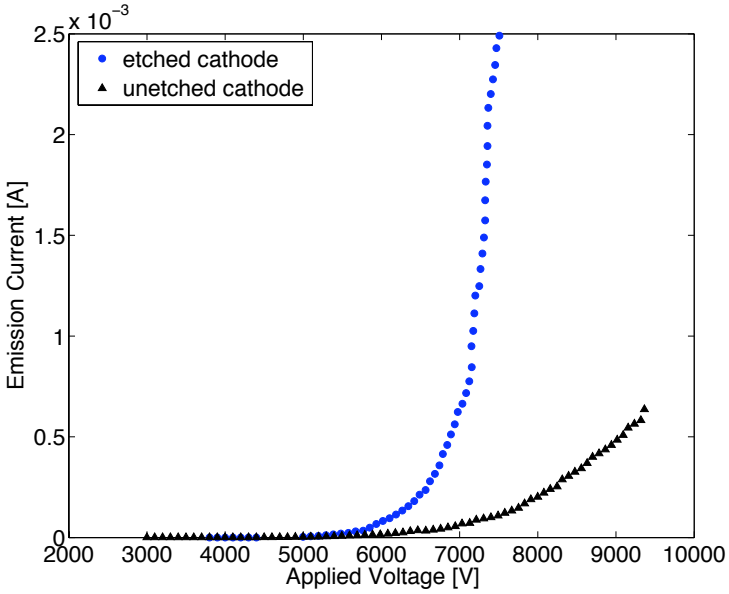

Figure 3.7: Plot showing the total emission current as a function of anode-cathode voltage from etched CKE4 cathode in comparison to unetched CKE4.

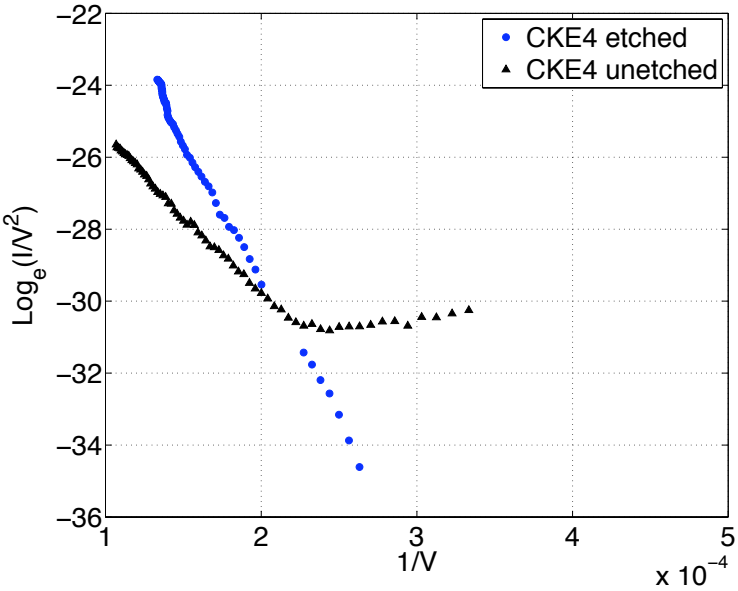

Figure 3.8: F-N plot comparison between etched and unetched CKE4 cathode

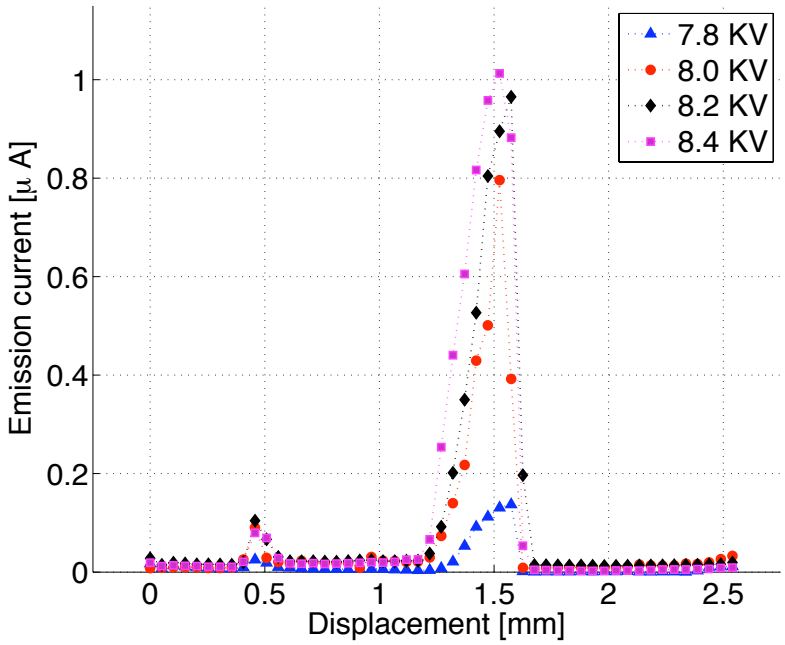

Figure 3.9: Lateral scan over CKE4 showing emission currents from locations along the scan at different voltages

detectable levels of thermal emission as seen from the unetched cathode. Further discussion on this is in the sub-section results and analysis. Following the more than one order of magnitude rise in emission current, the experiment to measure local emission currents was setup.

3.2.3 Experiment: Local emission current

The micro-aperture and Faraday cup collector along with the 3-axis cathode positioner can be used to measure local emission currents as described in chapter 2 page 20. The etched CKE4 cathode emitted currents that could be detected using this setup. The CKE4 cathode was moved in the lateral direction and electrons that pass through the micro-aperture were collected by the Faraday cup collector. The location of a raised ridge under the aperture was expected to result in higher current at the

collector and thus a plot of currents from different locations on a lateral dimension was expected to contain peaks at regular intervals. This was observed from such an experiment and a plot of emission currents from a lateral scan over the cathode at different voltages is shown in figure 3.9. From figure 3.9, two unequal peaks in emission current can be seen. These peaks in emission current are from the locations of knife edges on the CKE4 cathode, as can be seen from the distance between the peaks, which corresponds approximately to the distance between two knife edges on the cathode. The reason for unequal magnitudes of these peaks is amounted to the non-uniformity in knife edge thickness following the etching process. To check for this non-uniformity of emission along, lateral as well as transverse scans were done on a single knife edge. The resulting emission current map is seen in figure 3.10. This figure also shows the non-uniformity of emission current due to micro-structure present on the top of the knife edge.

3.2.4 Results & Analysis

It is evident from figure 3.7, that a higher aspect ratio and hence higher β due to etching has resulted in a higher emission current. However, the absence of previously observed thermal emission is intriguing. Our hypothesis is that the process of etching cleaned the surface of any oxides or other contaminants that might have led to an unusually low work function in CKE4. Although the work function extracted for CKE4 is unusually low, it still is comparable to the value extracted for a CKE cathode from the same batch by X. He [12] [22]. We believe that the process of etching, cleaned the surface of oxides and other contaminants as well as reduced the surface roughness, which was attributed to wire-EDM processing. It is known that reduction in surface roughness increases the work function [28]. Hence, as a result of etching, we produced a surface with a work function closer to the value of bulk copper, which is tabulated

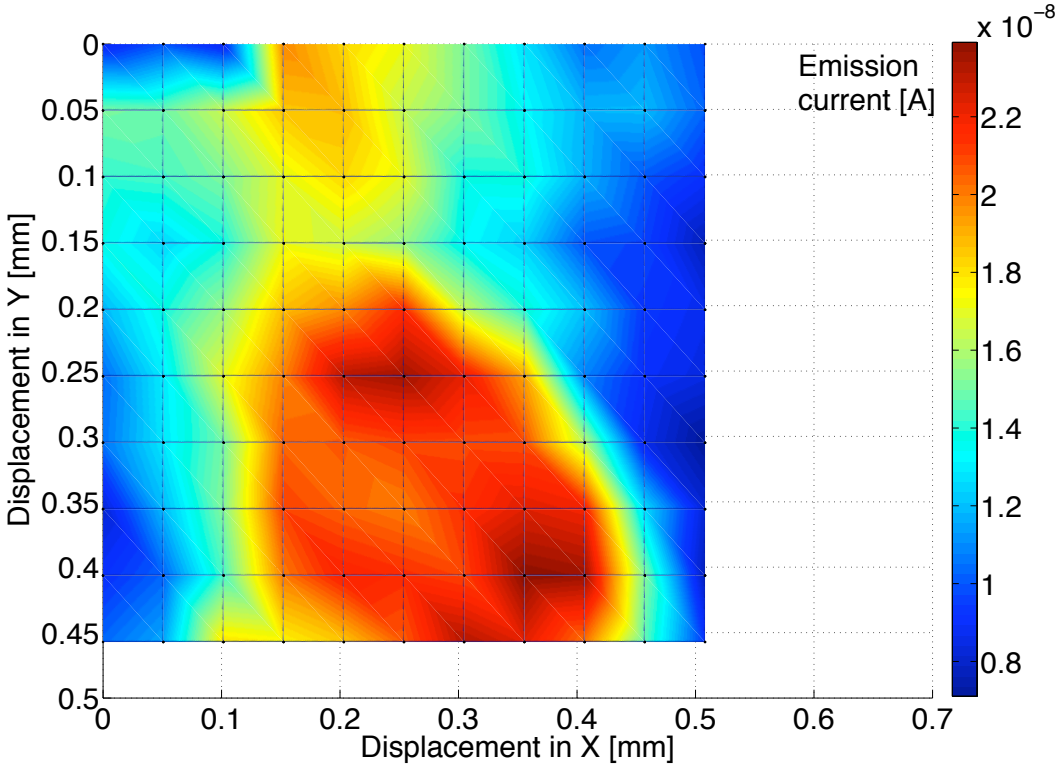

Figure 3.10: Plots show surface scan over CKE4 showing emission current distribution over the surface of a single knife edge

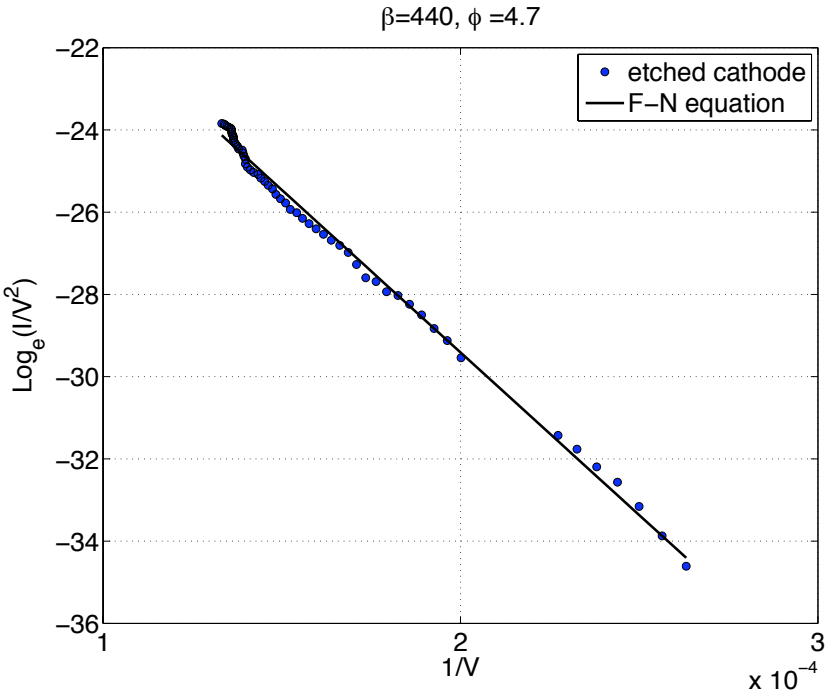

Figure 3.11: Calculating the β for the etched CKE4 cathode using work function, $\phi = 4.7$ eV, from the slope of the F-N plot

to be in the range of 4.48–4.94 eV[29] depending on the crystal face of copper surface. Using an average value of 4.7 eV, a value of β was calculated for the etched CKE4 cathode from the slope of the F-N plot as shown in figure 3.11. The resulting value of field enhancement factor, $\beta = 440$. This value is reasonable considering the aspect ratio of the knife edges.

Further, the emission area was extracted for the etched CKE4 cathode, again using Forbes' method, utilizing the assumed bulk copper work function and calculated β. Figure 3.13 shows the calculated variation of emitting area for etched CKE4 and the average emitting area found to be 6.3×10^{-7} m^2. This average value is very near to the area on top of the knife edges which is found to be 6.77×10^{-7} m^2. From the figure 3.13 it is also seen that the variation in emitting area as a function of applied field is almost linear and the slope is smaller than that for the unetched CKE4 cathode. A

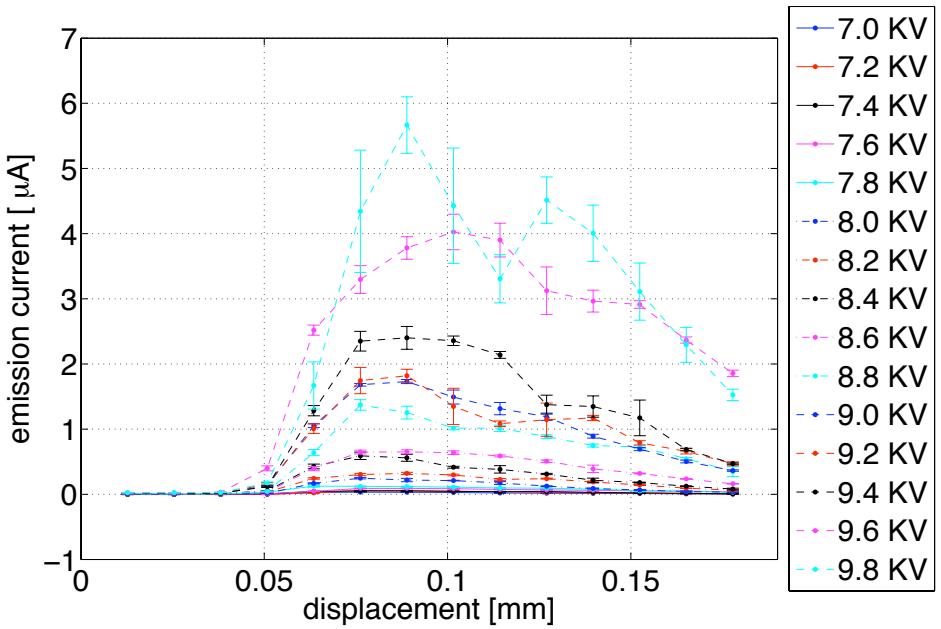

Figure 3.12: Emission current profile across one knife edge for etched CKE4

comparison of the variation in emitting area for both of these cathodes is shown in figure 3.14 and the difference in trends of variation as a function of applied voltage can be seen.

Additional experiments on measurement of local emission currents were done for a larger range of voltages (7 kV–10 kV) to analyze the variation of the peaks in emission current. Figure 3.12 shows the profile of emission current across one knife edge. In a simplistic model, as the applied voltage is raised, surface electric field increases and emission current. This higher current density spread over a larger area of emission and as a result the emission area increases. The highest or the peak of the profile of emission current signified electrons being emitted from the regions of highest field enhancement (assuming the work function to be uniform over the region) and summation of currents from different locations across the knife edge represent electrons coming from the complete top of the knife edge. Hence, a ratio of the total emission current from the knife edge, I_t, to the peak of emission current profile, I_p,

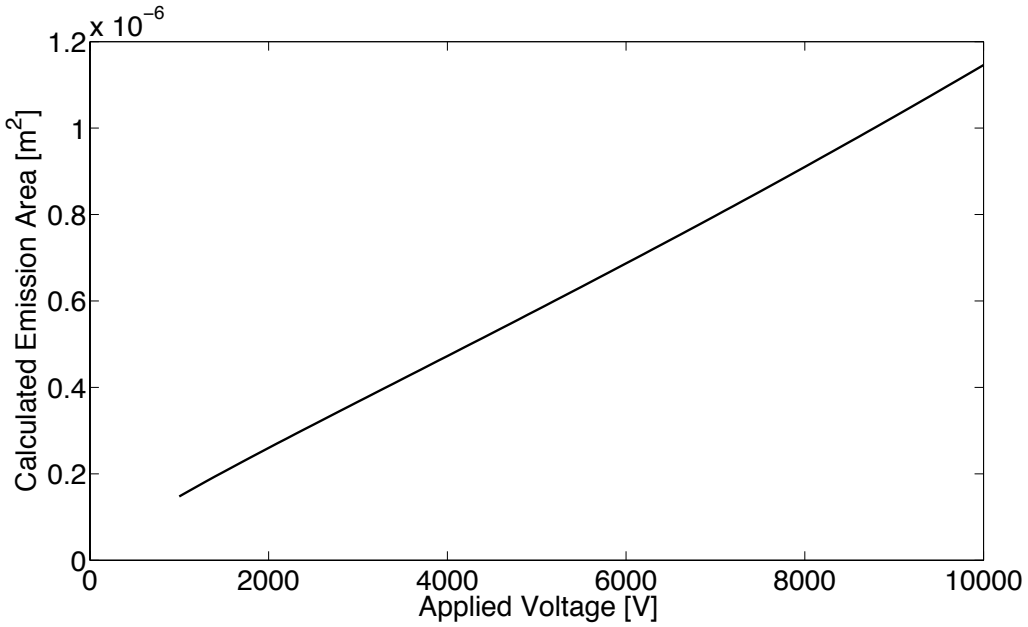

Figure 3.13: The variation of emitting area for etched CKE4 cathode as calculated using Forbes' method.

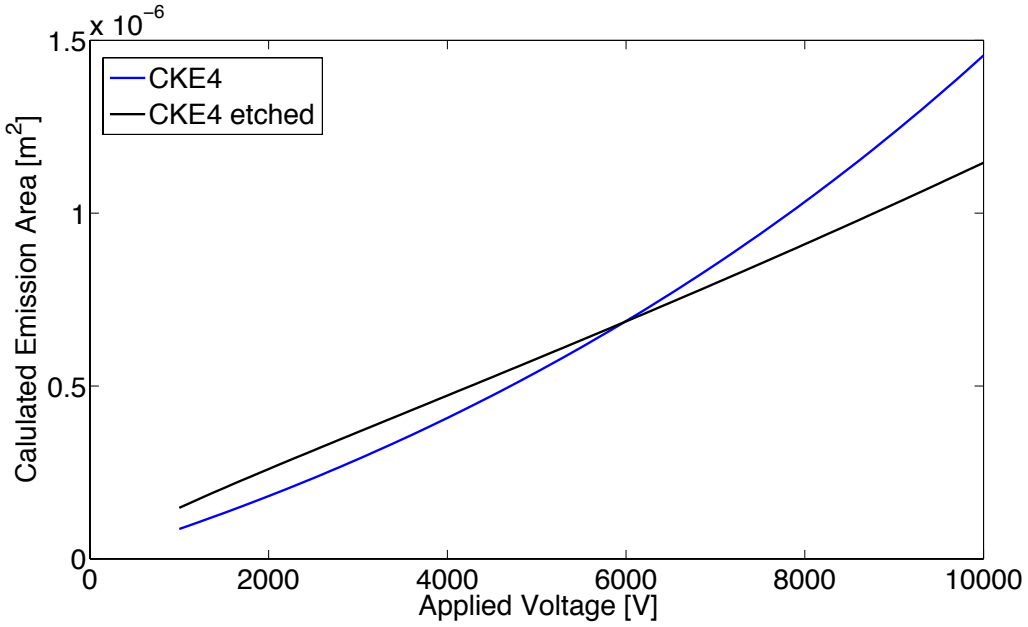

Figure 3.14: Comparison of calculated emitting area variation for CKE4 and etched CKE4 cathodes. The etched CKE4 cathode shows smaller variation in emitting area.

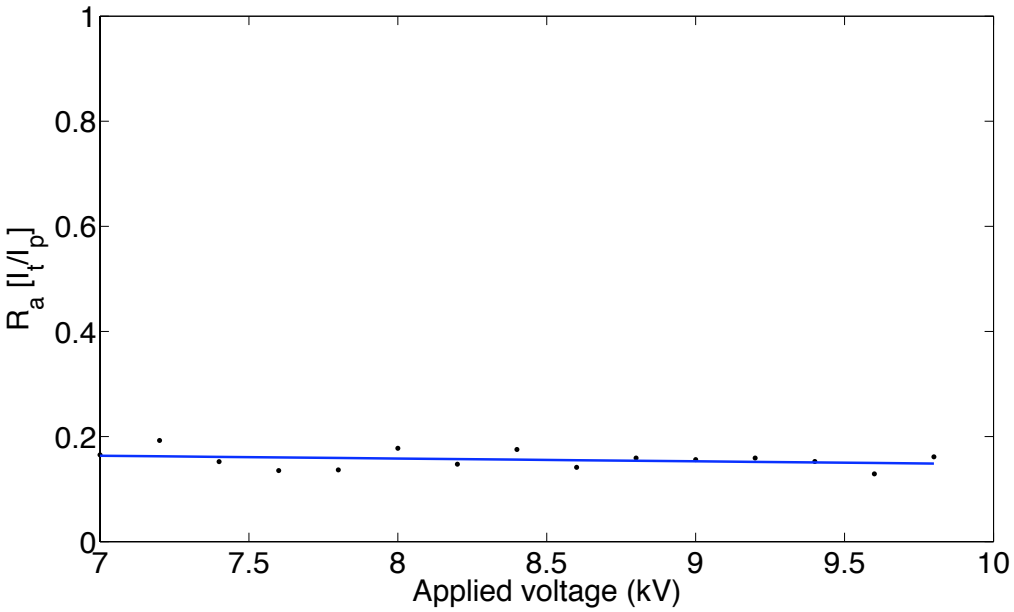

Figure 3.15: Plot of emission area ratio, R_a as a function of applied voltage over a range of 7 kV to 10 kV.

would represent the ratio of total emission area of the cathode to the actual emission area, R_a. Figure 3.15 shows a plot of this ratio, R_a, as a function of the voltage. It is seen that R_a drops only slightly from 0.2 to 0.13, signifying that the area of emission increases only slightly over the range of applied voltage from 7 kV to 10 kV. This is also seen from figure 3.13 which shows that from 7 kV to 10 kV the emitting area changes only from approximately 8×10^{-7} m^2 to 11×10^{-7} m^2.

To summarize, the table 3.1 displays the cathode parameters extracted from CKE4 before and after etching, showing a change in the work function, field enhancement factor and the effective emitting area, which is attributed to the process of etching. These calculated parameters show expected values and are reasonable for the cathodes considered in the experiments.

In the experiments with etched CKE4, a thermal emission regime could not be detected. This loss in detectable thermal emission currents was hypothesized to be

Cathode	β	ϕ [eV]	A [$\times 10^{-7}$m^2]
CKE4	400	2.96	6.66
CKE4 (etched)	440	4.7	6.3

Table 3.1: Summary of cathode parameters extracted from experimental data on CKE4 and CKE4-etched cathodes

due to an increase in work function as a result of surface cleansing from etching. So the next logical objective was to try and lower the work function of the surface of the etched CKE4 cathode to test whether detectable thermal emission currents are observed.

This objective was proposed to be accomplished by deposition of a thin film of a low work function, conductive material on top of the CKE cathodes. Since the CKE4 cathode surface showed an ambiguous change in work function from etching, it was decided to fabricate another batch of CKE cathodes. The geometry of the new set of CKE cathodes was exactly similar to the old ones except for the small change in the knife-edge width. The new CKE cathodes had a knife-edge thickness of around 100 microns compared to the 130 microns thickness in the old set of cathodes. The next chapter describes experiments done with the new set of CKE cathodes. It also includes a description of some important properties of Lanthanum hexaboride (LaB_6), which was used as a low work function thin film on the CKE cathodes, as well as the deposition technique.

Chapter 4

LaB_6 and new CKE cathode

Lathanum Hexaboride or LaB_6, is a low work function material, used extensively as an electron emitter both for thermal emission as well as field emission applications. This material was chosen for deposition over a new set of CKE cathodes to provide a low work function surface. This chapter describes properties of LaB_6 as a field emitter, the process of deposition of LaB_6 thin film over CKE cathode as well as the experiments and results with the new CKE cathodes.

4.1 Testing new CKE cathode

As mentioned in the previous chapter, the new set of CKE cathodes are fabricated, using the same process of wire-EDM and have the same geometry as the old batch except the difference in the knife edge width. The new CKE cathodes have nine knife-edges each with a width of $\sim$ 100 microns as compared to the $\sim$ 130 microns width in the previous batch. To ensure a clean copper surface, the new cathode was cleansed in a ultrasonic bath with ethanol and other solvents to remove oil, debris and other surface impurities. Further, the cathode is attached to its holder inside the vacuum chamber and baked at $>$ 200°C to remove moisture from the surface.

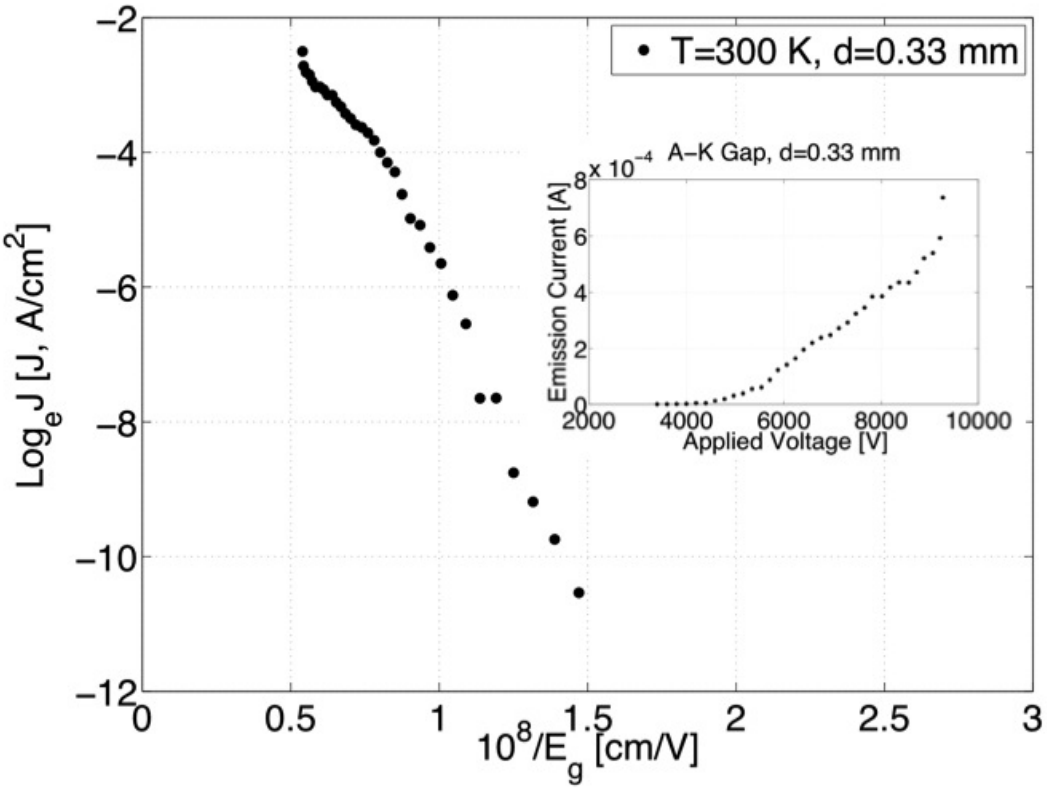

Figure 4.1: Modified F-N plot for the new CKE cathode showing deviation from nonlinearity which is hypothesized to be due to space charge effect in the small A-K gap of 0.33 mm. The inset shows a plot of emission current versus applied voltage.

After pumping down the vacuum chamber to $\sim 2\times10^{-9}$ Torr, and conditioning the cathode for more than $10,000$ shots, experiments to measure total emission current were performed. The results of those experiments are shown in figure 4.1. The inset in figure 4.1 shows a plot of emission current versus applied voltage for a anode-cathode (A-K) spacing, d of 0.33 mm. A deviation from linearity is seen for this smaller A-K spacing from figure 4.1. Our hypothesis is that this effect is due to space charge effects in the smaller A-K gap. The emission current and applied voltage data used for these plots have been corrected for the drop in voltage across the external measurement resistor and hence the most plausible explanation for the nonlinearity is due to space charge effects.

To support this hypothesis a comparison is with the theory of space charge effects in field emission is done and figure 4.1 is plotted in modified F-N coordinates which are $\ln J$ for the y-axis and $1/E_g \equiv d/V$ for the x-axis. These coordinates are used to compare the data directly with figure 4.2 from the Barbour et al paper [30]. In this plot of current density versus voltage, the curve ACE was calculated the standard F-N equation neglecting any space charge contribution. The curve BD is calculated from the Boguslavskii-Langmuir law (also known as the Child-Langmuir law) which is given by,

$$J = \frac{4}{9kd^2} \cdot V_a^{3/2}, \tag{4.1}$$

where $k = 2\pi(2m_e/e)^{1/2}$, d is the A-K spacing and V_a is the applied voltage. Then, the relationship between electric field, current density and the potential was found by integrating the Poisson equation for a potential distribution between infinite planar electrodes which is,

$$\frac{d^2V}{dx^2} = -k \cdot J \cdot V^{-1/2}. \tag{4.2}$$

with the boundary conditions that take the form,

$$V|_{x=0} = 0 \qquad V|_{x=d} = V_a \qquad dV/dx|_{x=0} = \mathbf{E}. \tag{4.3}$$

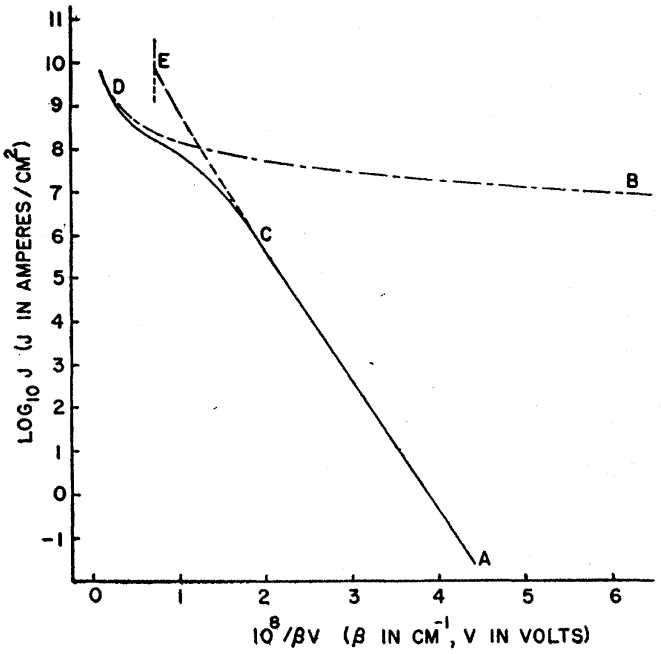

Figure 4.2: Theoretical dependance of current density with applied voltage including space charge effects [30].

The resulting equation was then solved in combination with the F-N equation to eliminate J and field strength in terms of applied potential is then given by,

$$4kaV_a^{3/2}\exp[-b/\mathbf{E}] - 3V_a = 9k^2a^2\mathbf{E}^2d^2\exp[-2b/\mathbf{E}] - 3\mathbf{E}d. \tag{4.4}$$

The F-N equation 1.12 and the above equation 4.4 can be used to calculate the current density for fixed values of electric field strength as a function of applied voltage which includes space charge effects. The curve ACD in figure 4.2 was calculated using these equations. It is seen that the initial part of the curve coincides with the F-N straight line and with increase in applied voltage, the curve asymptotically approaches the Boguslavskii-Langmuir curve.

The possibility of space charge limited emission from the CKE cathodes at smaller A-K spacing, implying higher electric fields, is an interesting proposition and further experiments could be planned to investigate this phenomenon in more detail.

4.2 Properties of LaB_6

LaB_6 is an inorganic chemical, bluish-purple in color and has semi-metallic properties. Lanthanum hexaboride crystallizes in a simple cubic lattice, with B_6-octahedra in body-centered positions and La ions at the corners of the unit cell. Two of the three electrons donated by the cation saturate the covalent bonds of the boron network, the third one is responsible for the high metallic conductivity (roughly one fifth of that of copper) of the material. In particular, a surface band is identified as a major source of the high electron yield that makes LaB_6 so useful for practical applications [31].

LaB_6 is known to be an excellent electron emitter and has been extensively used as a thermionic cathode since 1951 due to Lafferty [32]. Recently it has been investigated for field emission cathodes and found to be a good candidate for use in cold cathodes [33], [34], [35]. LaB_6 is a heavily researched and widely used material because of its physical properties like a strikingly low work function (2.6 eV), nature of low volatility, low resistance and very high melting point (2210 ℃) [36]. Since the commercial availability of LaB_6 cold cathodes, it has greatly improved the performance of electron-optic instruments like the scanning electron microscope and transmission electron microscope owing to small optical size of emitter, high brightness and most important, low electron energy spread.

The properties of LaB_6 thin-films have been shown to vary depending on the deposition conditions [37]. Different processes have been used for deposition such as pulsed laser deposition (PLD) [38], magnetron sputtering [39] and chemical vapor deposition [40]. The deposited thin film can be amorphous, polycrystalline or nearly single crystal depending on the deposition conditions and parameters. The most important condition for deposition is the substrate and the crystallinity of the LaB_6 film depends on this factor.

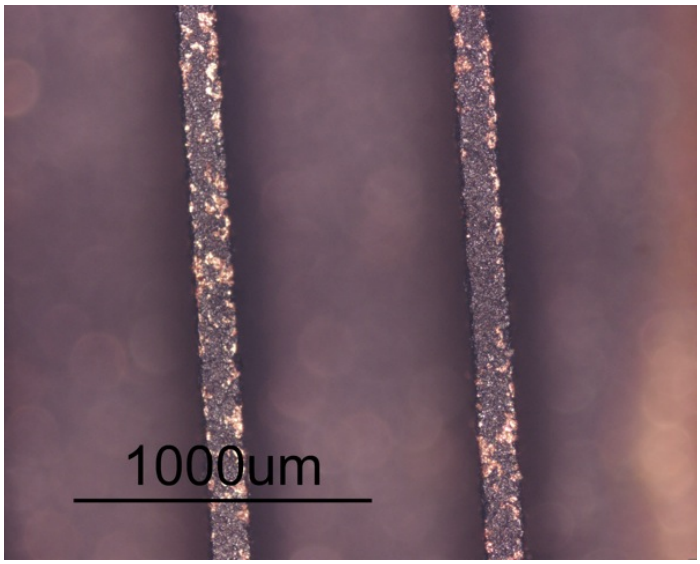

Figure 4.3: Optical microscope image of CKE cathode showing two knife edges. The LaB_6 thin-film is deposited by magnetron sputtering without substrate heating and adhesion layer. The thin-film is seen to be flaking off the surface of the knife edges because of poor quality and bonding.

4.3 Deposition of LaB_6

DC magnetron sputtering was chosen for deposition of LaB_6 on the CKE cathodes based on availability of equipment and literature reviews. The first deposition was done on a single 4 inch target Denton vacuum coating system employing DC magnetron sputtering at the Material Science Center in UW Madison. Substrate heating while deposition was not possible in this system. This deposition was at 200 V and 15 mTorr argon pressure for a duration of 42 minutes. The thickness of the LaB_6 thin-film was approximately 1 micron. However, it was observed that the quality of the deposited thin-film was very poor and the adhesion to the CKE cathode was also very poor. A picture of the deposited cathode is shown in figure 4.3. From this picture it is seen that the deposited thin-film is flaking off from spots on the knife edge and the surface is grainy.

Due to the poor quality of the deposited LaB_6 film, we decided to use a different sputtering system which would be capable of substrate heating as well as allow deposition of an adhesion layer without breaking vacuum. The Wisconsin Center for Applied Microelectronics (WCAM) provides a clean room facility with a sputtering deposition system capable of performing the tasks required for our LaB_6 thin-film deposition. This CVC 601 DC sputterer has two target holders and a rotating substrate base. Matt Kirley carried out these depositions. The first set of deposition was done with a 3 inch LaB_6 target. With this target size the substrate heater could not be operated and hence deposition was done at room temperature. Before deposition the CKE cathode was ultrasonically cleaned in a ethanol bath to remove surface impurities. Then, titanium was first deposited from a 6 inch target at 1000 W power and 3 mTorr argon pressure for 10 minutes. Subsequently, LaB_6 was deposited using a 3 inch target at 350 W power and 5 mTorr argon pressure for 30 minutes. The deposited film was about 1 micron in thickness. Figure 4.4 shows an image of the CKE cathode on which LaB_6 film was deposited. The quality of this film is seen to be better than the previous deposition without a Ti adhesion layer. The thin-film coating was also more robust and did not flake off the surface. This particular cathode is called CKE-LB1. Field emission experiments and their results for this cathode are described in the following section.

With a 3 inch LaB_6 target substrate heating could not be done. However, an elevated substrate temperature facilitates crystalline film formation. Thus, a 6 inch LaB_6 target was acquired and deposition was done on another CKE cathode utilizing the substrate heater as well as a Ti adhesion layer. In this deposition process, after sonicating the cathode, Ti adhesion layer was first deposited for 10 minutes at 1000 W power and 3 mTorr argon pressure. Then, LaB_6 was deposited using the 6 inch target for 30 mins at 700 W power and 5 mTorr argon pressure. The substrate was heated

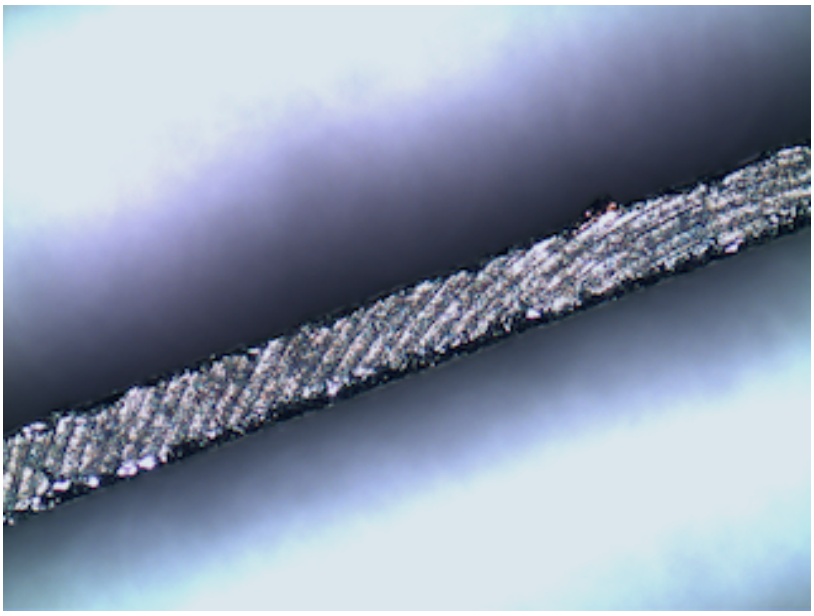

Figure 4.4: Optical microscope image of a CKE-LB1 knife edge with LaB_6 thin-film deposited from CVC 601 DC sputterer with Ti adhesion layer.

to approximately 200℃ by a radiative substrate heater. We call this cathode CKE-LB2. With the same procedure another CKE cathode was deposited with 4 of the 9 vanes masked with copper tape so that local emission current measurements could be done to compare emission from the copper side to the LaB_6 coated side without breaking vacuum to change cathodes. Additionally, this ensures that the geometric field enhancement factor on both sides is approximately same. We name this half coated cathode CKE-LB3. Figure 4.5 shows a picture of two vanes of the CKE-LB3 cathode. The one on the lower right is the masked side with bare copper and the upper left vane is coated with LaB_6 thin-film. The process of substrate heating while LaB_6 deposition shows the best quality thin-film. The experiments with CKE-LB2 and CKE-LB3 and their results are described in the following sections.

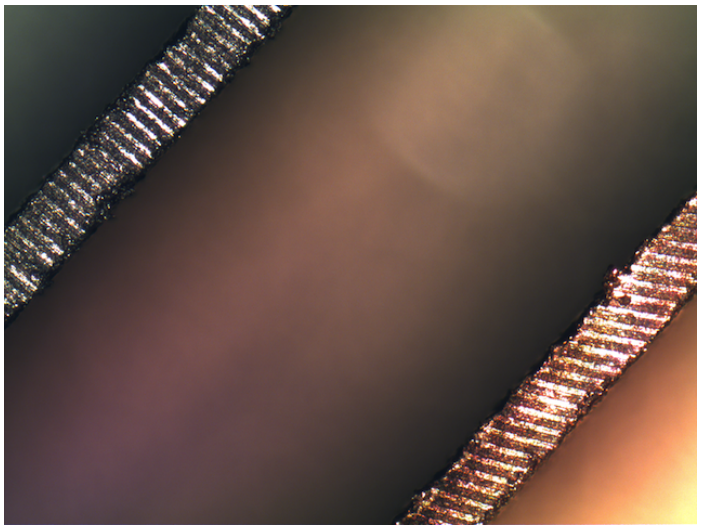

Figure 4.5: Optical microscope image of CKE-LB3 knife edge showing the lower right vane of bare copper and upper left vane coated with LaB_6 deposited on a heated substrate

4.4 Experiments on CKE-LB cathodes

This section describes the field emission experiments done with the CKE cathodes coated with a LaB_6 thin-film. The three cathodes differed in the deposition process. CKE-LB1 and CKE-LB2 differed in the use of heated substrate for the later. CKE-LB2 and CKE-LB3 followed the same deposition procedure, however, the later was masked such that only 5 of the 9 vanes were coated.

4.4.1 Experiments with CKE-LB1

An optical microscope image of CKE-LB1 is shown in figure 4.4. The deposition of Lab_6 for this cathode was done at room temperature. CKE-LB1 was prepared for field emission experiment to measure total emission current from the cathode following the same procedure for vacuum pump down and cathode conditioning as outlined in chapter 3. A series of experiments were performed at different temperatures,

keeping the A-K spacing at 0.33 mm to see the effect of temperature on the emission current. The temperature of the cathode is varied by heating the whole vacuum chamber using heating tape. The temperature is controlled using a variac to adjust the power input to the heating tape. A non-contact, infrared-radiation thermometer is used to accurately determine the temperature of the cathode. Along with varying the temperature another set of experiments were done by varying the A-K spacing to see the effect of varying surface electric field on the emission current. Significant nonlinearity in F-N coordinates is seen from emission at higher temperatures as shown and described in the results below.

4.4.2 Results for CKE-LB1

The figures 4.6 and 4.7 show the result of varying the temperature for a constant A-K spacing of 0.33 mm, in terms plots of emission current and applied voltage in I versus V co-ordinates and F-N co-ordinates, respectively. Figure 4.8 shows emission current versus applied voltage in terms of F-N plots for different A-K spacings, at a constant cathode temperature of 75℃.

The figure 4.8 shows that as the A-K gap decreases emission current increases as expected, due to higher electric field strength on the cathode. The plots in this figure are all linear even at high electric fields which shows that even at these higher voltages there is no space charge effect. This could partly be due to lower emission current density as compared to the bare CKE cathode (about 4 times lower emission current). Another reason could be that of a voltage drop across the LaB_6 film.

The important feature to note from the figure 4.7 is the nonlinearity of emission current in the F-N plots. Our hypothesis for explaining this nonlinearity is based on the nature of the LaB_6 thin-film. Since the deposition on CKE-LB1 was done at room temperature, the coating is assumed to be mostly amorphous in nature.

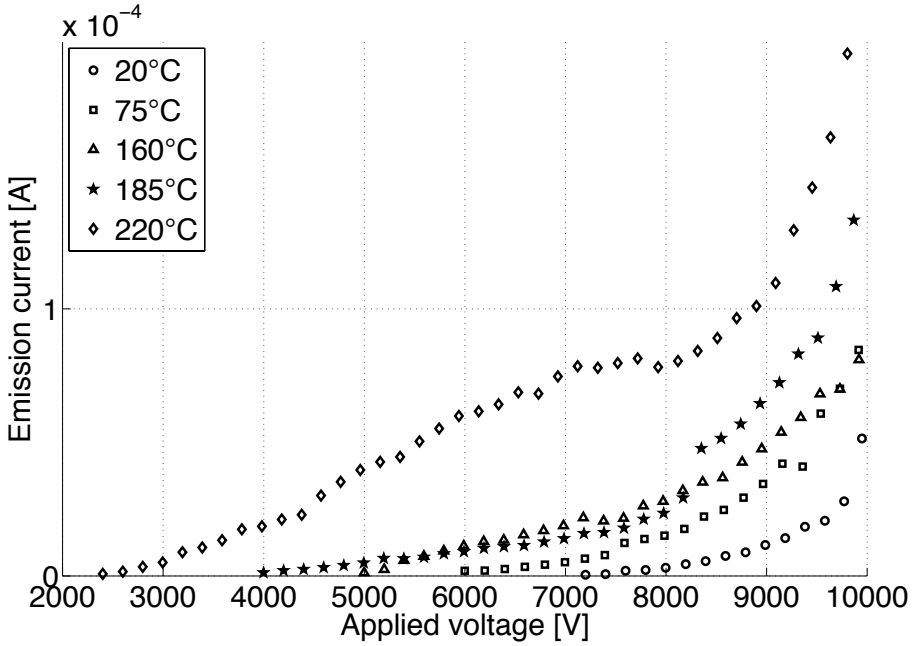

Figure 4.6: Emission current versus applied voltage for CKE-LB1 for various cathode temperatures.

The saturation in current at higher voltages and linear rise after a certain voltage is explained by our hypothesis based on the presumption of an amorphous, resistive LaB_6 thin-film. This hypothesis will be presented in the next section.

4.4.3 Experiments & results with CKE-LB2

CKE-LB2, as described above in section 1.3, was coated with LaB_6 at an elevated temperature of $\sim$ 200℃. With a heated substrate the sputtered atoms have more time to move around the substrate and hence form a better crystal structure than sputtering at room temperature. It was hence expected that CKE-LB2 would have at least have a poly-crystalline LaB_6 thin-film and this characteristic would have an effect on the field emission current characteristics.

With this expectation, similar total emission current measurement experiments

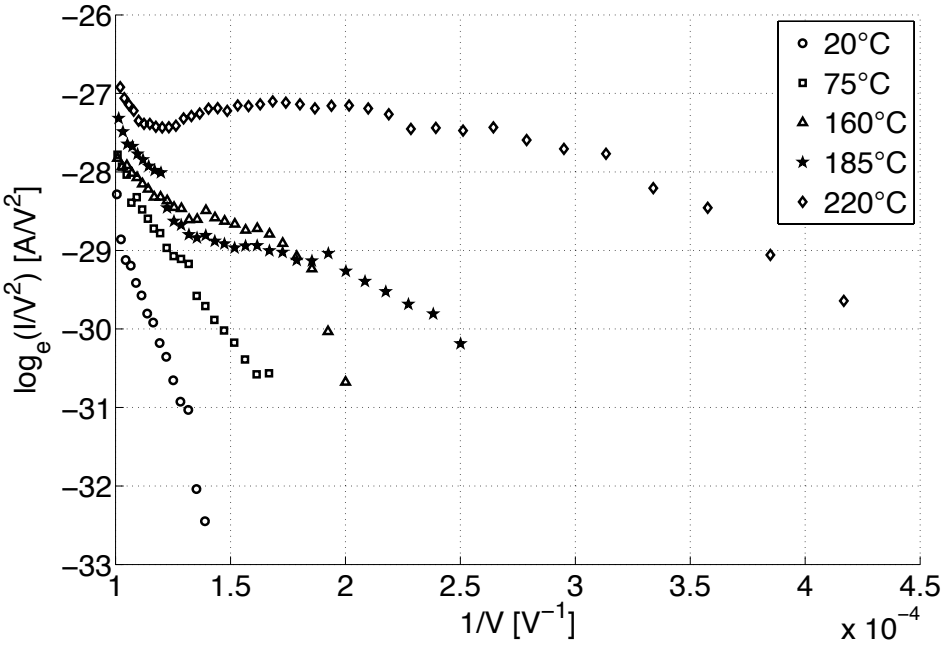

Figure 4.7: F-N plots of emission current and applied voltage for CKE-LB1 for various cathode temperatures.

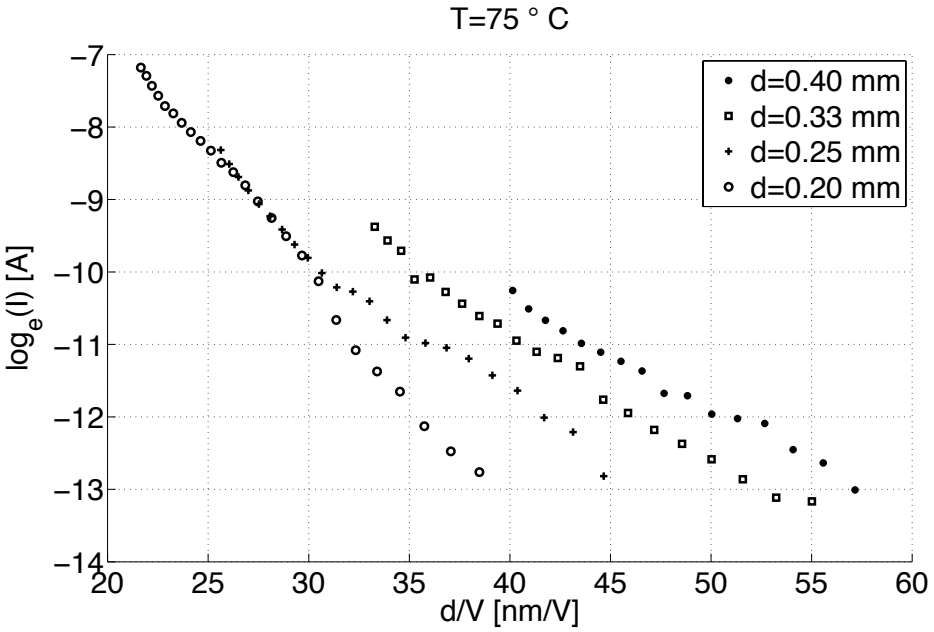

Figure 4.8: Emission current and applied voltage is plotted for CKE-LB1 for different A-K spacings at constant cathode temperature of 75°C.

were done with CKE-LB2. The experiments were done at two different temperatures, elevated ($\approx$ 185°C) and room temperature. The A-K spacing was 0.33 mm for these experiments. The results of these experiments are shown in figures 4.9 and 4.10.

Comparison of plots of CKE-LB1 and CKE-LB2 however offers more insight. Figures 4.12 and 4.11 and show this comparison. From these plots it is evident that the heated substrate deposition of LaB_6 thin-film leads to higher emission current, which is thought to be due to the increased crystallinity of the deposited film. The other prominent difference in field emission currents of CKE-LB1 and CKE-LB2 is the linearity of the F-N plot. It is seen that linearity of F-N plots, of the heated substrate deposited cathode is higher. Thus, observations from comparison leads to the following hypotheses explaining the differences which are both based on the presumption that room temperature deposition leads to a more amorphous LaB_6 thin-film, where as, heated substrate deposition leads to poly-crystalline LaB_6 thin-film.

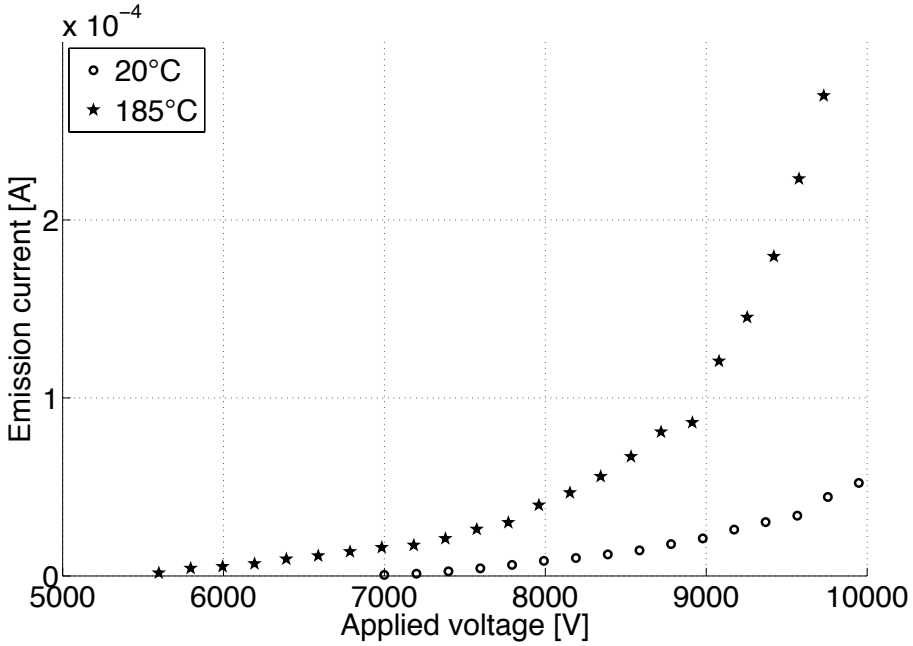

Figure 4.9: Emission current versus applied voltage for CKE-LB2 for different cathode temperatures.

4.5 Qualitative model of emission from LaB_6 CKE structure

In the field emission experiment results seen above, the following important points were observed. First, although LaB_6 has a much lower work function than copper, there is no significant increase in emission current. In fact, the emission current from the LaB_6 coated CKE cathode at the highest applied voltage is about an order of magnitude lower than emission current from bare CKE cathode. This is seen in figure 4.13, which shows a comparison of F-N plots for bare CKE cathode and the LaB_6 coated cathodes (CKE-LB1 and CKE-LB2). The second observation was that emission current from the CKE-LB cathodes increased at elevated temperatures, which was expected, due to the lower work function of LaB_6 assisting thermal-field emission. The third important observation is the nonlinearity in the FN plots. This is

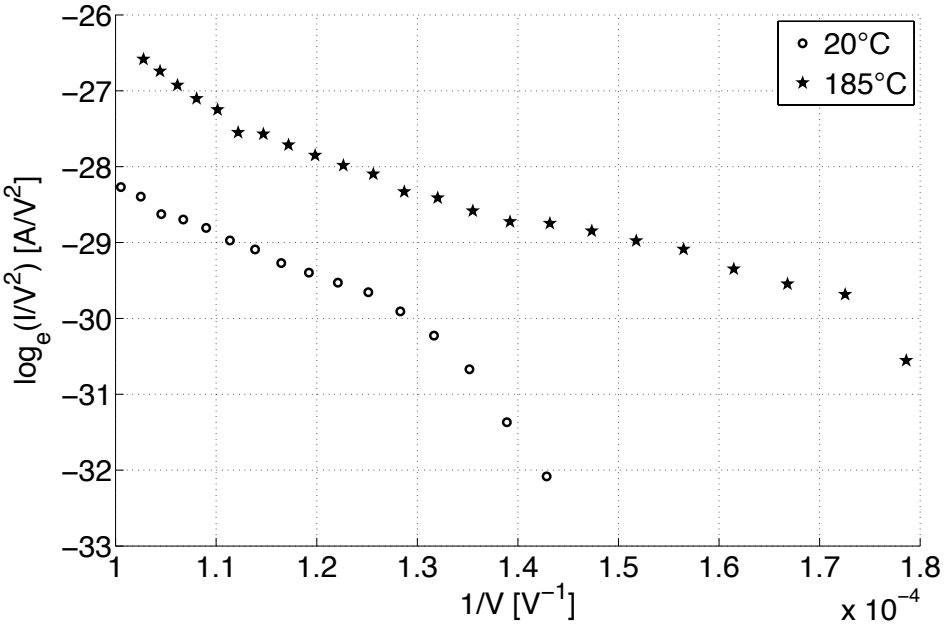

Figure 4.10: F-N plots of emission current and applied voltage for CKE-LB2 for different cathode temperatures.

seen in figure 4.14 from the F-N plot of CKE-LB1 at 220℃. It is seen from this figure that, the curve initially increases linearly and then saturates. Further by increasing the applied voltage after a certain voltage the curve starts increasing again. The fourth observation is that this nonlinearity seen in the F-N plots of CKE-LB1 is not prominent in F-N plots of CKE-LB2. The only difference in CKE-LB1 and CKE-LB2 is the temperature of the substrate at which the Ti adhesion layer and LaB_6 thin-film are deposited.

Thus, to explain these observations we have developed a hypothesis based on the assumption that the crystal structure of the LaB_6 thin-film deposited depends on the substrate temperature during deposition. The CKE-LB1 is assumed to have an amorphous LaB_6 film on it where as CKE-LB2, a poly-crystalline. By assuming an amorphous thin-film, we however, do not eliminate the possibility of small local domains (a few nm) that can have some atomic order and hence the possibility of "band

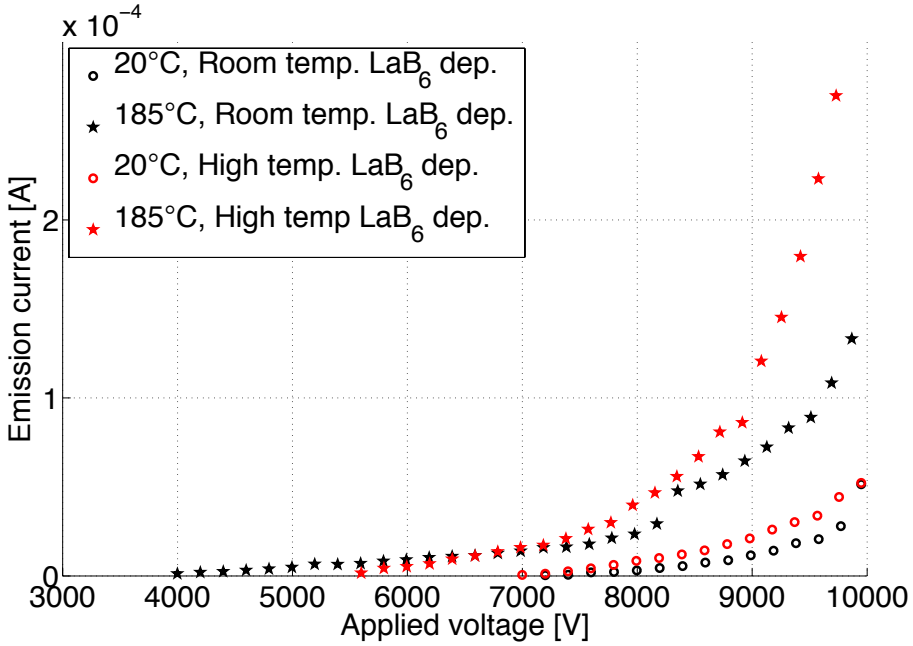

Figure 4.11: Emission current versus applied voltage for CKE-LB1 and CKE-LB2 compared as a function of different cathode temperatures.

structure effects". For poly-crystalline, we think of the film as having significantly larger domains of atomic order, such that the properties of this thin-film are closer to bulk LaB_6 crystal properties. Thus, the amorphous LaB_6 film is more resistive and has a wider variation in work function than the poly-crystalline LaB_6 film.

Apart from the resistivity in the LaB_6 film there are other effects that can influence electron transport from the metal into LaB_6. The electrons in the metal see a potential barrier at the interface of the metal-LaB_6 due to the difference in work functions (1.5 eV) as well as due to scattering because of the higher disorder in the amorphous LaB_6. Now, to explain why a low work function material (LaB_6) emits less electrons than copper, we propose the following.

When LaB_6 and the metal are brought together, the system goes to a thermodynamic equilibrium, much as n-type and p-type semiconductors in a pn-junction. Thus, the Fermi levels of these materials align. Since the metal as well as LaB_6 have

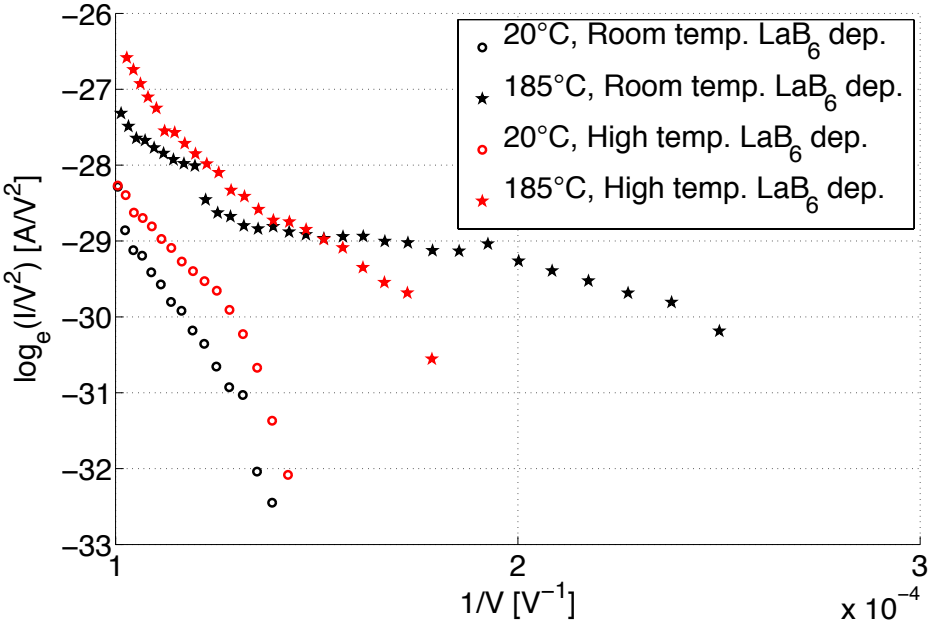

Figure 4.12: F-N plots of emission current and applied voltage for CKE-LB1 and CKE-LB2 compared for different cathode temperatures.

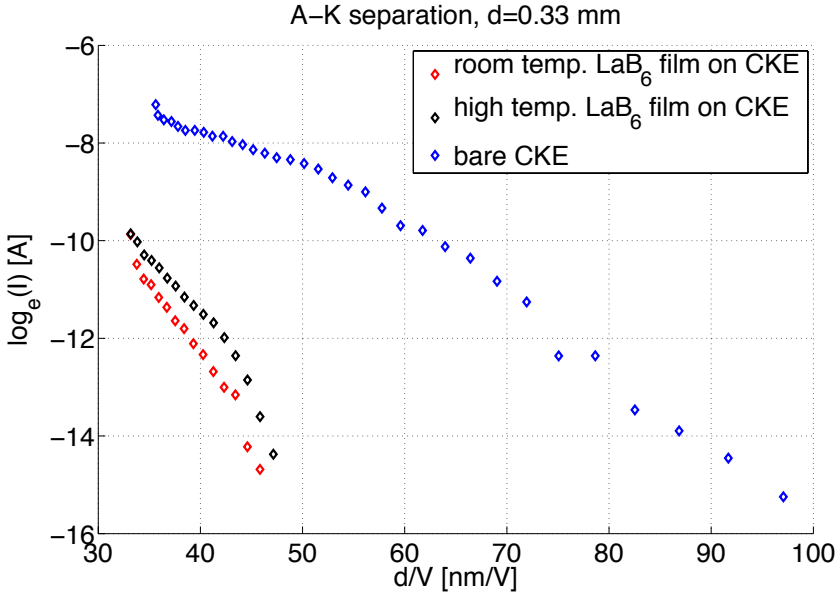

Figure 4.13: Comparison of F-N plots of field emission data from bare CKE cathode, CKE-LB1 and CKE-LB2 at room temperature.

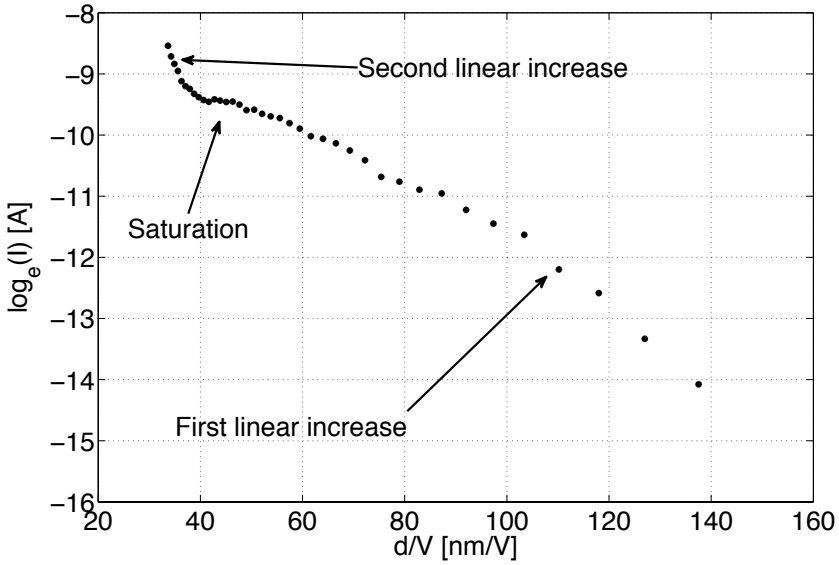

Figure 4.14: The nonlinearity in the F-N plot for CKE-LB1 field emission experiment at 220℃. Here, $d = 0.33$ mm.

Fermi-levels in the close vicinity of their conduction bands, the combined system should have a Fermi-level somewhere in between the individual levels. Furthermore, because of the amorphous nature of the LaB_6 film, this average level forms a band of energies. To bring about this thermodynamic equilibrium, some electrons from the LaB_6 would migrate to lower energies in the metal, making the metal band rise a bit and LaB6 band bend down at the interface. A qualitative band diagram is shown in figure 4.15. According to the Fermi distribution function, very few electrons would be available for conduction in the conduction band of LaB_6 as they would have energies greater than the Fermi-level of the system, corresponding to electrons in the tail of the Fermi-distribution function. In contrast there would be a high electron density in the conduction band of the metal as it lies below the system Fermi-level.

Based on the above hypothesis, when applied voltage is low, the width of the potential barrier at the LaB_6-vacuum interface is narrowed by the surface enhanced

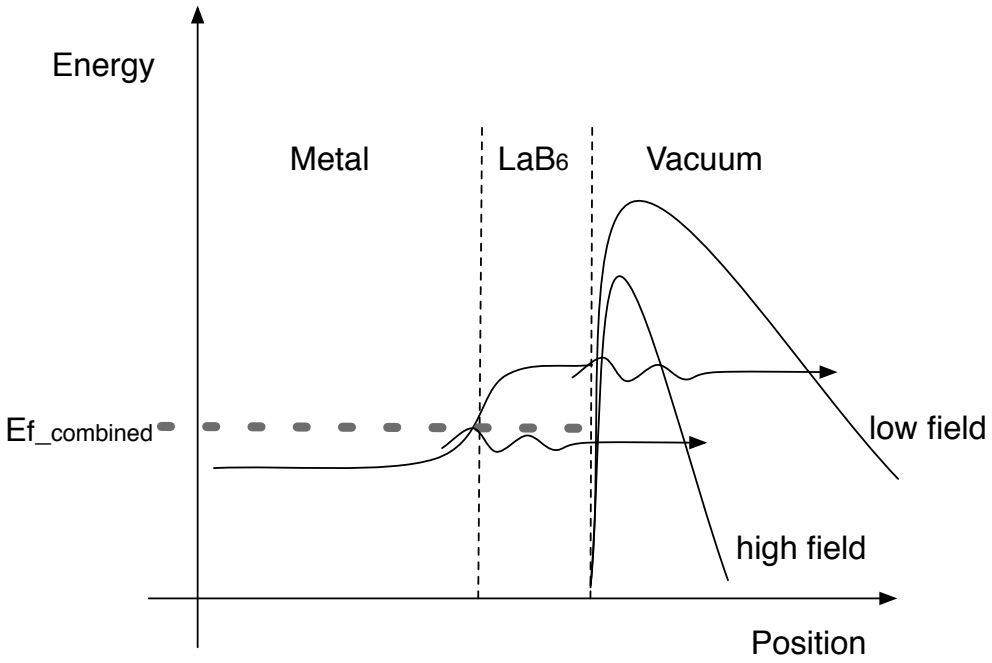

Figure 4.15: A qualitative energy band diagram for the metal-LaB_6-vacuum system.

electric field, enabling the possibility of tunneling of electrons from the LaB_6 conduction band states into vacuum. This emission results in the first linear increase seen in figure 4.14. However, since only few electrons (present in the tail of Fermi distribution) are available, the emission current is lower as compared to emission from bare copper, even though the work function of LaB_6 is low.

By increasing the applied voltage (hence the surface electric field), the emission current increases. However, more electrons tunnel out from the LaB_6 film than can be generated. This increase in emission current can also have an effect of increasing the IR voltage drop across the film. In the LaB_6, all this results in depletion of carriers and thus a saturation in the emission current, also seen in the experimental data in figure 4.14. The depletion of carriers in LaB_6 results in an effective +ve charge and electron accumulation at the metal-LaB_6 interface in an effective $-$ve charge. These induced charges induce an internal field, which modifies the barrier at the metal-LaB_6

interface by lowering it.

As the applied voltage is increased further, this internal barrier is lowered further, resulting in increased probability for electrons to cross this barrier into the LaB_6 film. Moreover, by further increasing the surface electric field, the barrier at the vacuum interface is further narrowed which also increases the probability for electrons in the conduction states of the metal to directly tunnel into vacuum, which could be possible for a thin LaB_6 film. Since now there is a higher electron density available for tunneling, the emission increases sharply and we see the second linear rise in current (figure 4.14).

Thus, overall field emission is affected by internal electron transport at the metal-LaB_6 interface, resistivity of the LaB_6 thin-film and even the possibility of field penetration in LaB_6. Together these effects can give rise to nonlinear field emission as observed in our experiments. Also, higher emission at higher temperatures can easily be explained by the fact that the Fermi distribution will allow more electrons in the distribution tail at higher temperatures to tunnel in the low applied voltage regime. Hence, the larger current at lower voltages results in higher IR drop across the film and a more prominent saturation effect as observed in the experiments.

Our hypothesis is that at low voltages, electrons are emitted via field emission from the LaB_6 surface, and electrons are replenished by conduction through the LaB_6, provided by the high density of conduction electrons from the copper. As the applied voltage (electric field) is increased, the IR voltage drop across the LaB_6 increases, and as a result, there is a diminishing returns effect. This essentially means that, as applied voltage is increased, less and less of it is actually available to increase the field emission because more and more of it is being sacrificed in the IR voltage drop across the LaB_6 film. Most of this IR voltage drop is assumed to occur at the copper-LaB_6 interface because of the difference in work functions of these two materials. This

explains the observation of saturation in the emission current with increasing applied voltage.

Now, for the poly-crystalline LaB_6 thin-film (CKE-LB2), since the conductivity is higher, IR voltage drop in the film is lower and hence the current saturation is lower at the same voltages. However, the potential barrier at the interface is not affected as much by the crystallinity of the LaB_6 film. Thus, with a more crystalline LaB_6 film, it is predicted that there would still be nonlinear field emission effect however it would be smaller compared to the amorphous LaB_6 film. This explains the CKE-LB2 F-N plot being more linear in the same voltage range (see figure 4.12). In this hypothesis, we have ignored any effects that could be due to the Cu-Ti interface. This is justified because Cu and Ti have almost the same work function and Ti is deposited under vacuum after cleaning the Cu surface.

Nonlinear field emission observations have been observed in semiconductors [41] and the most probable cause for such emission is the limited carrier generation rate in the bulk and other interrelated processes [42]. The hypothesis presented here is able to explain the nonlinear field emission observations in our experiments from bare CKE, room temperature deposited LaB_6 (CKE-LB1) and high temperature deposited LaB_6 (CKE-LB2) cathodes. To verify the hypothesis however, further experiments must be done to quantify the difference in emission from these different surfaces and estimate the resistivity of the LaB_6 thin film. Also, experiments have be done to confirm the difference in work functions for LaB_6 thin-film deposited on Cu with a Ti adhesion layer. These experiments can be done on cathodes in which half of the vanes are bare and the other half are coated, such as CKE-LB3.

Chapter 5

Summary & Conclusion

This chapter provides a summary of the experiments and results described in previous chapters. Future research directions and experiments are also suggested. Finally a conclusion to end the thesis.

5.1 Summary

Field emission is a process of electron emission by the process of quantum mechanical tunneling. Background theory of field emission including thermal-field emission is described in chapter 1. The field emission experiments described in this thesis were done in the vacuum electronics lab with the modified MACX system. This system, as described in chapter 2 is capable of local emission current as well as total emission current measurement. The experiments were done using copper knife-edge structures also described in chapter 2. In the preliminary experiments on the CKE cathode (CKE4), experimental data is used to extract cathode parameters β, ϕ and A. The procedure for extraction of these parameters and the experiments are described in chapter 3. Local emission current measurements are also done on the preliminary CKE cathode that was etched to increase the field enhancement factor.

The next set of experiments were done on a new set of CKE cathodes. The bare CKE cathode showed space charge limited field emission at smaller (< 0.33 mm) A-K spacing. Subsequently, LaB_6 was deposited by DC magnetron sputtering on the new CKE cathodes. LaB_6 is a semi-metal with a low bulk work function and is used as an electron emitter in number of applications. LaB_6 properties and deposition procedure is described in chapter 4. Chapter 4 also describes the experiments and results of LaB_6 thin-films deposited with the substrate at room (CKE-LB1) and at an elevated temperature (CKE-LB2). Nonlinear F-N plots are observed and their characteristics are shown to differ for these two cathodes. In the last part of chapter 4, a hypothesis for a qualitative model of field emission from the CKE-LB cathodes is put forth to explain the observed results.

5.2 Future experiments

A number of directions for future research can be suggested based on the results and observations in this research. The first further experiments can be done to explore thermal-field emission and refining the procedure of independently and unambiguously extracting cathode parameters using thermal emission regime for work function extraction and field emission regime for extracting field enhancement factor. The MACX system could be modified to sustain higher temperatures thus enabling thermal-field emission experiments at higher temperatures. The second research direction is to explore space charge limited emission for these CKE cathodes. The effect of A-K spacing on space charge limited emission can be investigated in more detail and the possibility of using space charge limited regime for cathode parameter extraction can be explored.

The most interesting research, however, is to investigate field emission from LaB_6 thin-films on conducting structures. Examining the effect of substrate heating on

the field emission characteristics can be studied in more detail. Different deposition techniques can also be experimented with such as e-beam evaporation and CVD. To verify the hypothesis presented in chapter 4, experiments can be done to compare local emission currents from a cathode, half coated with LaB_6. From this comparison an estimate of the LaB_6 thin-film resistivity can be determined. Independent work function measurements could be done to verify the LaB_6 film work function. Finally other cathode geometries could be considered as substrate for the LaB_6 films to enhance field emission.

5.3 Conclusion

High efficiency, low energy spread and bright electron sources are crucial for a number of important applications as mentioned in chapter 1. Field emission cathodes are very good candidates for these applications due to the high efficiency of the process of tunneling and other advantages. Therefore, the development of stable and high current density cold cathodes is crucial for the development of these applications. One of the applications that has recently gained a lot from field emission is that of vacuum microelectronics [43]. Several types of cathodes have been researched as electron sources, such as, carbon nanotubes/nano clusters. However, there is still much to be desired from these cathodes in terms of stability. LaB_6 is a material that has an unusually low work function and is a promising candidate for fabricating stable high current density field emitters.

The research presented in this thesis was directed towards this goal of developing stable high current density cold cathodes through examining extraction of cathode parameters as well as investigating new materials and structures such as LaB_6 coated knife edge structures for field emission, however, a number of questions still remain unanswered. A robust, easily manufacturable and economical cathode like the LaB_6

coated CKE cathode is a very good model system to study and understand the physics of field emission. Combined with the MACX setup we hope to further this field with additional research and experiments.

Bibliography

[1] J. I. Gersten and F. W. Smith, *The Physics and Chemistry of Materials*. Wiley, illustrated ed., 2001.

[2] K. L. Jensen, "General thermal-field emission equation," *Applied physics letters*, vol. 88, April 2006.

[3] R. W. Wood, "A new form of cathode discharge and the production of x-rays, together with some notes on diffraction. preliminary communication," *Phys. Rev. (Series I)*, vol. 5, pp. 1–10, Jul 1897.

[4] R. H. Fowler and L. Nordheim, "Electron emission in intense electric fields," *Proc. R. Soc. London, Ser A*, vol. 119, March 1928.

[5] E. L. Murphy and R. H. Good, "Thermionic emission, field emission, and the transition region," *Phys. Rev.*, vol. 102, June 1956.

[6] R. D. Young, "Theoretical total-energy distribution of field-emitted electrons," *Phys. Rev.*, vol. 113, pp. 110–114, Jan 1959.

[7] R. Gomer, *Field emission and field ionization*. Springer, reprint, illustrated ed., 1993.

[8] R. G. Forbes, "Physics of generalized fowler-nordheim-type equations," *J. Vac. Sci. Technol. B*, vol. 26, April 2008.

[9] O. W. Richardson, *The emission of electricity from hot bodies*. Longmans, Green and co., 2 ed., 1921.

[10] S. O. Pillai, *Solid State Physics*. New Age International, 6 ed., 2005.

[11] K. L. Jensen, "Electron emission theory and its application: Fowler-nordheim equation and beyond," *J. Vac. Sci. Technol. B*, vol. 21, Jul/Aug 2003.

[12] X. He, *Measurement, Modeling and Analysis of cold cathodes*. PhD thesis, University of Wisconsin, Madison, 2008.

[13] X. He, J. Scharer, J. Booske, and S. Sengele, "One-dimensional combined field and thermionic emission model and comparision with experimental results," *J. Vac. Sci. Technol. B*, vol. 26, April 2008.

[14] G. P. Gilfoyle, "A new teaching approach to quantum mechanical tunneling," *Computer physics communications*, vol. 121, pp. 573–577, September 1999.

[15] K. L. Jensen, "Field emitter arrays for plasma and microwave source applications," *Phys. Plasmas*, vol. 6, no. 5, pp. 2241–2253, 1999.

[16] S. H. Gold and G. S. Nusinovich, "Review of high-power microwave source research," *Review of Scientific Instruments*, vol. 68, no. 11, pp. 3945–3974, 1997.

[17] E. W. Muller, "Work function of tungsten single crystal planes measured by the field emission microscope," *Journal of Applied Physics*, vol. 26, no. 6, pp. 732–737, 1955.

[18] D. den Engelsen, "The temptation of field emission displays," *Physics Procedia*, vol. 1, no. 1, pp. 355 – 365, 2008. Proceedings of the Seventh International Conference on Charged Particle Optics (CPO-7).

[19] K. Aplin, B. Kent, W. Song, and C. Castelli, "Field emission performance of multiwalled carbon nanotubes for a low-power spacecraft neutraliser," *Acta Astronautica*, vol. 64, no. 9-10, pp. 875 – 881, 2009.

[20] R. Miller, Y. Y. Lau, and J. Booske, "Electric field distribution on knife-edge field emitters," *Applied physics letters*, vol. 91, August 2007.

[21] T. E. Stern, R. S. Gossling, and R. H. Fowler, "Further studies in the emission of electrons from cold metals," *Proc. R. Soc. London, Ser A*, vol. 124, pp. 699–723, July 1929.

[22] X. He, J. Scharer, J. Booske, and S. Sengele, "Modelling of cold emission cathode by inclusion of combined field and thermionic emission processes," *Journal of Applied Physics*, vol. 102, September 2007.

[23] B. Ha and C. J. Lee, "Electronic structure and field emission properties of in situ potassium-doped single-walled carbon nanotubes," *Applied Physics Letters*, vol. 90, pp. 023108–+, Jan. 2007.

[24] S. C. Lim, H. J. Jeong, K. S. Kim, I. B. Lee, D. J. Bae, and Y. H. Lee, "Extracting independently the work function and field enhancement factor from thermal-field emission of multi-walled carbon nanotube tips," *Carbon*, vol. 43, no. 13, pp. 2801 – 2807, 2005.

[25] R. G. Forbes, "Simple good approximations for the special elliptic functions in standard fowler-nordheim tunneling theory for a schottky-nordheim barrier," *Applied Physics Letters*, vol. 89, no. 11, p. 113122, 2006.

[26] R. G. Forbes, "Field emission: New theory for the derivation of emission area from a fowler-nordheim plot," vol. 17, pp. 526–533, AVS, 1999.

[27] O. Cakir, "Review of etchants for copper and its alloys in wet etching processes," *Key Engineering Materials*, vol. 364, pp. 460–465, 2008.

[28] W. Li and D. Y. Li, "On the correlation between surface roughness and work function in copper," *The Journal of Chemical Physics*, vol. 122, no. 6, p. 064708, 2005.

[29] P. O. Gartland, S. Berge, and B. J. Slagsvold, "Photoelectric work function of a copper single crystal for the (100), (110), (111), and (112) faces," *Phys. Rev. Lett.*, vol. 28, pp. 738–739, Mar 1972.

[30] J. P. Barbour, W. W. Dolan, J. K. Trolan, E. E. Martin, and W. P. Dyke, "Space-charge effects in field emission," *Phys. Rev.*, vol. 92, pp. 45–51, Oct 1953.

[31] R. Monnier and B. Delley, "Properties of lab_6 elucidated by density functional theory," *Phys. Rev. B*, vol. 70, p. 193403, Nov 2004.

[32] J. M. Lafferty, "Boride cathodes," *Journal of Applied Physics*, vol. 22, p. 299, 1951.

[33] H. Zhang, J. Tang, Q. Zhang, G. Zhao, G. Yang, J. Zhang, O. Zhou, and L. Qin, "Field emission of electrons from single lab_6 nanowires," *Advanced Materials*, vol. 18, pp. 87–91, 2006.

[34] D. J. Late, M. A. More, D. S. Joag, P. Misra, B. N. Singh, and L. M. Kukreja, "Field emission studies on well adhered pulsed laser deposited lab_6 on w tip," *Applied Physics Letters*, vol. 89, no. 12, p. 123510, 2006.

[35] X. Wang, Z. Lin, K. Qi, Z. Chen, Z. Wang, and Y. Jiang, "Field emission characteristics of lanthanum hexaboride coated silicon field emitters," *Journal of Physics D: Applied Physics*, vol. 40, no. 16, pp. 4775–4778, 2007.

[36] Y. G. Gogotsi and R. A. Andrievski, *Materials Science of Carbides, Nitrides and Borides*, vol. 68. Springer, 1999.

[37] W. Waldhauser, C. Mitterer, J. Laimer, and H. Stori, "Structure and electron emission characteristics of sputtered lanthanum hexaboride films," *Surface & Coatings Technol.*, vol. 74, pp. 890–896, 1995.

[38] V. Craciun and D. Craciun, "Pulsed laser deposition of crystalline lab6 thin films," *Applied Surface Science*, vol. 247, no. 1-4, pp. 384 – 389, 2005. Proceedings of the European Materials Research Society 2004 - Symposium N.

[39] C. Mitterer, H. M. Ott, J. Komenda-Stallmaier, P. Schmölz, W. S. M. Werner, and H. Störi, "Sputtered decorative hard coatings within the system lab6—zrb2," *Journal of Alloys and Compounds*, vol. 239, no. 2, pp. 183 – 192, 1996.

[40] S. S. Kher and J. T. Spencer, "Chemical vapor deposition of metal borides: 7. the relatively low temperature formation of crystalline lanthanum hexaboride thin films from boron hydride cluster compounds by chemical vapor deposition," *Journal of Physics and Chemistry of Solids*, vol. 59, no. 8, pp. 1343 – 1351, 1998.

[41] G. Fursey, "Early field emission studies of semiconductors," *Applied Surface Science*, vol. 94-95, pp. 44 – 59, 1996. Proceedings of the 42nd International Field Emission Symposium.

[42] G. N. Fursey, *Field emission in vacuum micro-electronics.* Springer, 2005.

[43] G. N. Fursey, "Field emission in vacuum micro-electronics," *Appl. Surf. Science*, vol. 215, pp. 113–134, 2003.